

NOE and PGSE NMR Spectroscopic Studies of Solution Structure and Aggregation in Metallocenium Ion-Pairs

Cristiano Zuccaccia,^{†,‡} Nicholas G. Stahl,[†] Alceo Macchioni,^{*,‡} Ming-Chou Chen,[†] John A. Roberts,[†] and Tobin J. Marks^{*,†}

Contribution from the Department of Chemistry, Northwestern University, Evanston, Illinois 60208-3113, USA, and Dipartimento di Chimica, Università di Perugia, 06123, Perugia, Italy

Received September 25, 2003; E-mail: t-marks@northwestern.edu; alceo@unipg.it

Abstract: The solution structures of the metallocenium homogeneous polymerization catalyst ion-pairs [Cp₂ZrMe]⁺[MeB(C₆F₅)₃]⁻ (**1**), [(1,2-Me₂Cp)₂ZrMe]⁺[MeB(C₆F₅)₃]⁻ (**2**), [(Me₂SiCp₂)ZrMe]⁺[MeB(C₆F₅)₃]⁻ (**3**), [Me₂C(Fluorenyl)(Cp)ZrMe]⁺[FPBA]⁻ (FPBA = tris(2,2',2''-nonafluorobiphenyl)fluoroaluminate) (**4**), [*rac*-Et(Indenyl)₂ZrMe]⁺[FPBA]⁻ (**5**), [(Me₅Cp)₂ThMe]⁺[B(C₆F₅)₄]⁻ (**6**), [(Me₂SiCp₂)Zr(Me)(THF)]⁺[MeB(C₆F₅)₃]⁻ (**7**), [(Me₂SiCp₂)Zr(Me)(PPh₃)]⁺[MeB(C₆F₅)₃]⁻ (**8**), [(Me₂SiCp₂)Zr(Me)(THF)]⁺[B(C₆F₅)₄]⁻ (**9**), [(Me₂Si(Me₄-Cp)(*t*-BuN)Zr(Me)(solvent)]⁺[B(C₆F₅)₄]⁻ (solvent = benzene, toluene) (**10**), [(Cp₂ZrMe)₂(*μ*-Me)]⁺[MePBB]⁻ (PBB = tris(2,2',2''-nonafluorobiphenyl)borane) (**11**), and [(Cp₂Zr)₂(*μ*-CH₂)(*μ*-Me)]⁺[MePBB]⁻ (**12**), having the counteranion in the inner (**1**, **3**, **4**, **5**, and **6**) or outer (**7**, **8**, **9**, **10**, **11**, and **12**) coordination sphere, have been investigated for the first time in solvents with low relative permittivity such as benzene or toluene by ¹H NOESY and ¹H, ¹⁹F HOESY NMR spectroscopy. It is found that the average interionic solution structures of the inner sphere contact ion-pairs are similar to those in the solid state with the anion B-Me (**1**, **3**) or Al-F (**5**) vectors oriented toward the free zirconium coordination site. The HOESY spectrum of complex **6** is in agreement with the reported solid-state structure. In contrast, in outer sphere contact ion-pairs **7**, **8**, **9**, and **10**, the anion is located far from the Zr-Me⁺ moiety and much nearer to the Me₂Si bridge than in **3**. The interionic structure of **8** is concentration-dependent, and for concentrations greater than 2 mM, a loss of structural localization is observed. PGSE NMR measurements as a function of concentration (0.1–5.0 mM) indicate that the tendency to form aggregates of nuclearity higher than simple ion-pairs is dependent on whether the anion is in the inner or outer coordination sphere of the metallocenium cation. Complexes **2**, **3**, **4**, **5**, and **6** show no evidence of aggregation up to 5 mM (well above concentrations typically used in catalysis) or at the limit of saturated solutions (complexes **3** and **6**), while concentration-dependent behavior is observed for complexes **7**, **8**, **10**, and **11**. These outer sphere ion-pairs begin to exhibit significant evidence for ion-quadruples in solutions having concentrations greater than 0.5 mM with the tendency to aggregate being a function of metal ligation and anion structure. Above 2 mM, compound **8** exists as higher aggregates that are probably responsible for the loss of interionic structural specificity.

Introduction

It is now well-known that ion-pairing phenomena play a fundamental role in the performance of single-site group 4 metallocenium olefin polymerization catalysts. Numerous examples exist where cation–anion interactions substantially affect catalyst activity, stability, polymerization selectivity,^{1,2} and the microstructural properties of the resulting polyolefins.³ In addition, dianionic cocatalysts have been shown to enforce spatial confinement between two catalyst centers, allowing the production of LLDPE (linear low-density polyethylene) from a single ethylene feed.^{3c} The stereochemistry of single-site-derived

polymers is also known to be strongly affected by ion-pairing, while the nature of the influence depends on the chemical and structural properties of the cationic and anionic moieties. Thus, the stereoregularity of polypropylene produced by C_s- or C₁-symmetric catalysts is modulated via ion-pairing strength effects on the relative rates of olefin insertion to catalyst stereochemical inversion.^{3a,d,e} In contrast, the stereorigid systems based on *rac*-

[†] Northwestern University.

[‡] Università di Perugia.

(1) For recent reviews of single-site olefin polymerization, see: (a) Gibson V. C.; Spitzmesser, S. K. *Chem. Rev.* **2003**, *103*, 283 (b) Pedoutour, J.-N.; Radhakrishnan, K.; Cramail, H.; Deffieux, A. *Macromol. Rapid Commun.* **2001**, *22*, 1095. (c) Gladysz, J. A., Ed. *Chem. Rev.* **2000**, *100* (special issue on "Frontiers in Metal-Catalyzed Polymerization"). (d) Marks, T. J.; Stevens, J. C., Eds. *Top. Catal.* **1999**, *15* and references therein. (e) Britovsek, G. J. P.; Gibson, V. C.; Wass, D. F. *Angew. Chem., Int. Ed. Engl.* **1999**, *38*, 428. (f) Kaminsky, W.; Arndt, M. *Adv. Polym. Sci.* **1997**, *127*, 144. (g) Bochmann, M. *J. Chem. Soc., Dalton Trans.* **1996**, 255.

(2) For recent examples of catalyst–activator interplay see: (a) Metz, M. V.; Sun, Y.; Stern, C. L.; Marks, T. J. *Organometallics* **2002**, *21*, 3691 and references therein. (b) Chen, Y.-X.; Kruper, W. J.; Roof, G.; Wilson, D. R. *J. Am. Chem. Soc.* **2001**, *123*, 745. (c) Zhou, J.; Lancaster, S. J.; Walter, D. A.; Beck, S.; Thornton-Pett, M.; Bochmann, M. *J. Am. Chem. Soc.* **2001**, *123*, 223. (d) Chase, P. A.; Piers, W. E.; Patrick, B. O. *J. Am. Chem. Soc.* **2000**, *122*, 12911. (e) Chen, Y.-X.; Marks, T. J. in ref 1b, p 1391. (f) Metz, M. V.; Schwartz, D. J.; Stern, C. L.; Nickias, P. N.; Marks, T. J. *Angew. Chem., Int. Ed.* **2000**, *39*, 1312.

(3) (a) Mohammed, M.; Nele, M.; Al-Humydi, A.; Xin, S.; Stapleton, R. A.; Collins, S. *J. Am. Chem. Soc.* **2003**, *125*, 7930. (b) Li, L.; Metz, M. V.; Li, H.; Chen, M.-C.; Marks, T. J.; Liable-Sands, L.; Rheingold, A. L. *J. Am. Chem. Soc.* **2002**, *124*, 12725 and references therein. (c) Abramo, G. P.; Li, L.; Marks, T. J. *J. Am. Chem. Soc.* **2002**, *124*, 13966. (d) Chen, M.-C.; Marks, T. J. *J. Am. Chem. Soc.* **2001**, *123*, 11803. (e) Chen, M.-C.; Roberts, J. A. S.; Marks, T. J. *J. Am. Chem. Soc.*, in press. (d) Chen, M.-C.; Roberts, J. A. S.; Marks, T. J. *Organometallics*, in press.

C_2 -symmetric *ansa*-metallocenes with homotopic sites are less sensitive to the nature of the cocatalyst as manifested in the microstructure of the resulting polymer.⁴ Finally, as proposed by Busico and co-workers,⁵ strong anion association with the “mobile” active cation in “oscillating metallocene catalysts”⁶ can play a role analogous to that of the covalent bridge in *ansa*-metallocenes.

Although the phenomenological observation of ion-pairing effects is well recognized, the detailed connections between the catalyst/cocatalyst interplay and polymerization activity are still not completely understood. For example, it is not clear whether cocatalyst effects are exerted in the ground or transition state of “ $L_2M(\text{olefin})R^+$ ” species. Landis and co-workers⁷ used heavy-atom kinetic isotope effects to determine the nature of the transition state in 1-hexene homopolymerization catalyzed by *rac*-[$C_2H_4(1\text{-Indenyl})_2$]ZrMe₂ with various cocatalysts. They demonstrated the following: (1) the transition state in which alkene is committed to irreversible insertion into the growing polymer does not change significantly as a function of cocatalyst, (2) the alkene binding to the metal center is reversible, and (3) the dramatic effect of the cocatalyst structure on reaction rate arises from counteranion effects on the alkene association equilibrium constant and consequently, on the ground state. Seemingly in contrast, Bochmann⁸ and co-workers used quenched-flow propylene polymerization kinetic studies to demonstrate that, even in the presence of essentially identical numbers of active sites, i.e. in conditions of similar ground-state energies, the activation energetics of the chain growth are strongly modulated by the counteranion properties, implying a model in which the ion-pair is the actual propagating species. In the same work, the authors also suggested that anion exchange within higher-order ion-pair aggregates may provide a low-energy pathway for monomer binding, so that ion-quadruples or even higher aggregates may be the actual propagating species.

In this scenario it is clear that direct structural characterization of the cation–anion interactions in solution (i.e., in the medium in which these catalysts actually function) would greatly facilitate the basic mechanistic understanding of these complex systems. Although numerous X-ray diffraction,⁹ NMR spectroscopic,¹⁰ and theoretical¹¹ studies have been carried out to elucidate metallocenium ion-pair structure and dynamics, there is a paucity of direct experimental solution-phase metrical information concerning relative cation–anion positions. Even

less is known about interionic structure during the olefin enchainment and propagation processes.^{11,12}

In the past few years, it has been demonstrated that the solution-phase interionic structures of transition metal–organic ion-pairs can be successfully defined by combining information derived from NOE (nuclear Overhauser effect)¹³ and PGSE (pulsed field gradient spin–echo)¹⁴ NMR experiments. Semi-quantitative or quantitative NOE experiments allow deduction of the relative anion–cation positions and orientations (when both moieties are unsymmetrical). PGSE experiments provide an estimate of the average volume of the ionic species present and, consequently, the aggregation tendency.

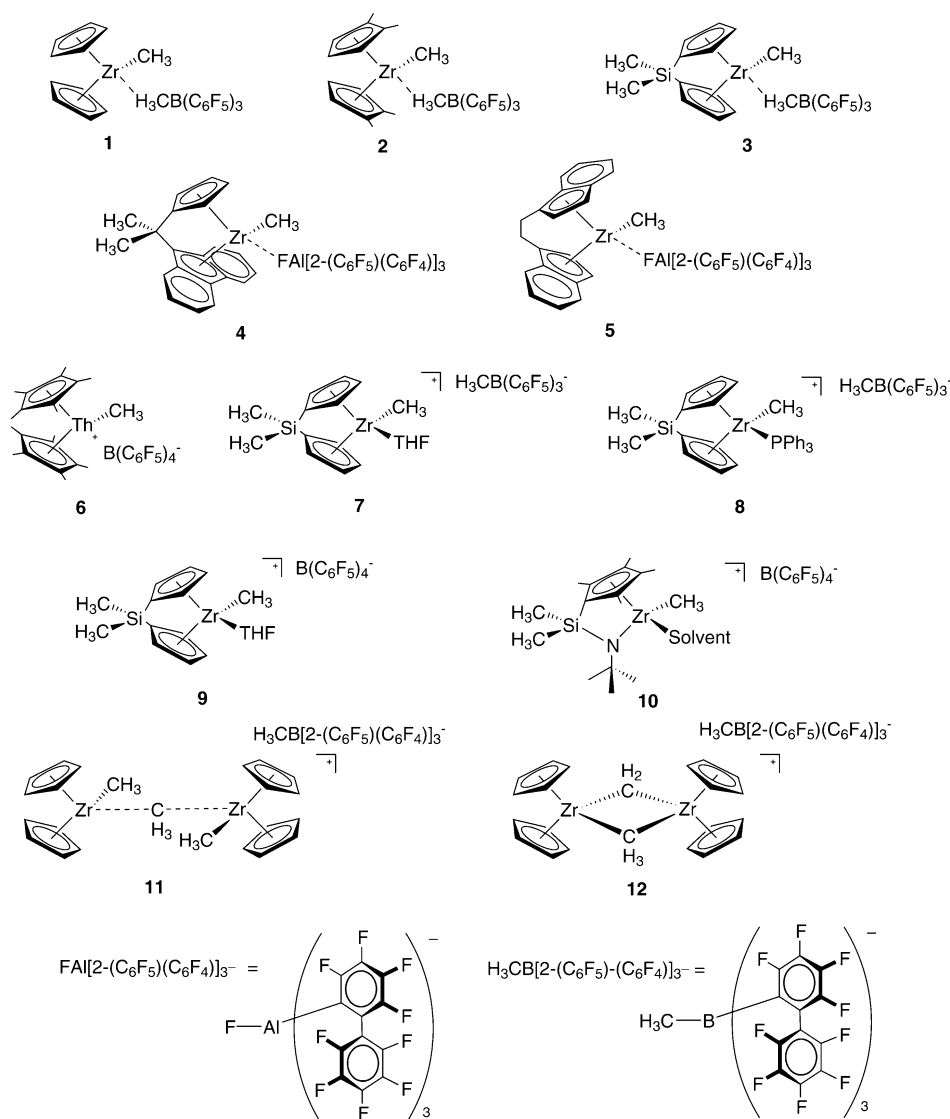
With the principal aim of better understanding metallocenium ion-pair structure–reactivity relationships, we have investigated a wide range of metallocenium ions by modifying the metal ligation as well as the structure of the weakly coordinating counteranion. Both ion-pairs in which the counteranion occupies one of the metal coordination sites (an inner sphere ion-pair, ISIP) and ion-pairs in which the counteranion is displaced from the first coordination sphere (an outer sphere ion-pair, OSIP) have been investigated. In ISIPs, the cation–anion interaction is primarily electrostatic in nature¹¹ but still possesses some coordinative character in that the anion occupies one of the otherwise formally vacant coordination sites of the cationic metal center. Recent calculations by Lanza and co-workers^{11a,c} and by Ziegler and co-workers^{11d} suggest a single concerted step for olefin uptake and insertion. In this case an ISIP can be considered to be one of the most experimentally accessible models for the catalyst during turnover. OSIPs represent contact ion-pairs in which the coordinatively saturated first coordination sphere of the cation is no longer accessible to the anion, and as a consequence, the anion is relegated to the second coordination sphere, interacting with the cation through electrostatic and other weak forces (H-bonding, π – π , CH– π , etc.) only. In the classical two-step Cossee-type mechanism,¹⁵ the outer sphere ion-pair can be considered to be a model to simulate the structural characteristics of the active site.

Preliminary results on the aggregation behavior in benzene solution of a limited series of isolable metallocenium ISIPs by a colligative method (freezing point depression) and by PGSE NMR have been recently reported by some of us.¹⁶ The results are consistent with a structural model for homogeneous metallocenium Ziegler–Natta polymerization catalysts consisting of a metal cation paired with a weakly coordinating anion to form an intimate 1:1 ion-pair in which aggregation is not detectable. Here we report a far more detailed ¹H NOESY, ¹⁹F, ¹H HOESY, and PGSE NMR investigation of a broad series of both ISIP (Chart 1) and OSIP metallocenium salts differing in metal, ancillary ligation, and counteranion in toluene-*d*₈ and

- (4) Resconi, L.; Cavallo, L.; Fait, A.; Piemontesi, F. in ref 1c, p 1253.
 (5) (a) Busico, V.; Van Axel Castelli, V.; Aprea, P.; Cipullo, R.; Segre, A.; Talarico, G.; Vacatello, M. *J. Am. Chem. Soc.* **2003**, *125*, 5451. (b) Busico, V.; Cipullo, R.; Kretschmer, W. P.; Talarico, G.; Vacatello, M.; Van Axel Castelli, V. *Angew. Chem., Int. Ed. Engl.* **2002**, *41*, 505.
 (6) (a) Lin, S.; Waymouth, R. M. *Acc. Chem. Res.* **2002**, *35*, 765. (b) Coates, G. W.; Waymouth, R. M. *Science* **1995**, *267*, 217.
 (7) Landis, C. L.; Rosaen, K. A.; Uddin, J. *J. Am. Chem. Soc.* **2002**, *124*, 12062.
 (8) Song, F.; Cannon, R. D.; Bochmann, M. *J. Am. Chem. Soc.* **2003**, *125*, 7641.
 (9) For recent examples see: (a) Metz, M. V.; Schwartz, D. L.; Stern, C. L.; Marks, T. J. *Organometallics* **2002**, *21*, 4159. (b) Liu, Z.; Somsook, E.; Landis, C. L. *J. Am. Chem. Soc.* **2001**, *123*, 2915. (c) Chen, E. Y.-X.; Kruper, W. J.; Roof, G.; Wilson, D. R. *J. Am. Chem. Soc.* **2001**, *123*, 745. (d) Bazan, G. C.; Cotter, W. D.; Komon, Z. J. A.; Lee, R. A.; Lachicotte, R. J. *J. Am. Chem. Soc.* **2000**, *122*, 1371. (e) Stephan, D. W.; Stewart, J. C.; Guérin, F.; Spence, R. E. v. H.; Xu, W.; Harrison, D. G. *Organometallics* **1999**, *18*, 116. (f) Bochmann, M.; Lancaster, S. J.; Hursthouse, M. B.; Malik, K. M. A. *Organometallics* **1994**, *13*, 2235.
 (10) (a) Beswick, C. L.; Marks, T. J. *J. Am. Chem. Soc.* **2000**, *122*, 10358. (b) Deck, P. A.; Beswick, C. L.; Marks, T. J. *J. Am. Chem. Soc.* **1998**, *120*, 1772. (c) Chen Y.-X.; Metz, M. V.; Li, L.; Stern, C. L.; Marks, T. J. *J. Am. Chem. Soc.* **1998**, *120*, 6287. (d) Chen, Y.-X.; Stern, C. L.; Marks, T. J. *J. Am. Chem. Soc.* **1997**, *119*, 2582.

- (11) (a) Lanza, G.; Fragalà, I. L.; Marks, T. J. *Organometallics* **2002**, *21*, 5594. (b) Vranka, K.; Ziegler, T. *Organometallics* **2001**, *20*, 905. (c) Lanza, G.; Fragalà, I. L.; Marks, T. J. *J. Am. Chem. Soc.* **2000**, *122*, 12764. (d) Chan, M. S. W.; Ziegler, T. *Organometallics* **2000**, *19*, 5182. (e) Fusco, R.; Longo, L.; Proto, A.; Masi, F.; Garbasi, F. *Macromol. Rapid Commun.* **1998**, *19*, 257. (f) Fusco, R.; Longo, L.; Masi, F.; Garbasi, F. *Macromol. Rapid Commun.* **1997**, *18*, 433.
 (12) (a) Stoebenu, E. J.; Jordan R. F. *J. Am. Chem. Soc.* **2003**, *125*, 3222. (b) Landis, C. R.; Rosaen, K. A.; Sillars, D. R. *J. Am. Chem. Soc.* **2003**, *125*, 1710.
 (13) Macchioni, A. *Eur. J. Inorg. Chem.* **2003**, 195 and references therein.
 (14) Binotti, B.; Macchioni, A.; Zuccaccia, C.; Zuccaccia, D. *Comments Inorg. Chem.* **2002**, *6*, 417.
 (15) Cossee, P. *J. Catal.* **1964**, *3*, 80.
 (16) Stahl, N. G.; Zuccaccia, C.; Jensen, T. R.; Marks, T. J. *J. Am. Chem. Soc.* **2003**, *125*, 5256.

Chart 1



benzene-*d*₆ solutions at room temperature over significant concentration ranges. The results of the NMR studies on the ISIP and OSIP complexes are presented in sequence.

Experimental Section

Materials and Methods. All manipulations of air-sensitive materials were performed with rigorous exclusion of oxygen and moisture in flamed Schlenk-type glassware on a dual-manifold Schlenk line, interfaced to a high-vacuum line (10⁻⁵ Torr), or in a nitrogen-filled MBraun glovebox with a high-capacity recirculator (<1 ppm O₂ and H₂O). All solvents were freeze-pump-thaw degassed on the high-vacuum line, dried over Na/K alloy, and vacuum-transferred to a dry storage tube having a PTFE valve. B(C₆F₅)₃ was a gift from Dow Chemical and was purified by recrystallization from pentane and vacuum sublimation. PPh₃ was purchased from Aldrich and purified by vacuum sublimation. [Cp₂ZrMe]⁺[MeB(C₆F₅)₃]⁻ (**1**),¹⁷ [(1,2-Me₂-Cp)₂ZrMe]⁺[MeB(C₆F₅)₃]⁻ (**2**),^{10b} [(Me₂SiCp₂)ZrMe]⁺[MeB(C₆F₅)₃]⁻ (**3**),¹⁸ [Me₂C(Fluorenyl)(Cp)ZrMe]⁺[FPBA]⁻ (FPBA = tris(2,2',2''-nonafluorobiphenyl)fluoroaluminate) (**4**),¹⁹ [*rac*-Et(Indenyl)₂ZrMe]⁺-

[FPBA]⁻ (**5**),^{10c} [(Me₅Cp)₂ThMe]⁺[B(C₆F₅)₄]⁻ (**6**),²⁰ [(Me₂Si(Me₄Cp)(*t*-BuN)Zr(Me)(Solvent)]⁺[B(C₆F₅)₄]⁻ (**10**),²⁰ and [(Cp₂ZrMe)₂(μ-Me)]⁺[MePBB]⁻ (PBB = tris(2,2',2''-nonafluorobiphenyl)borane) (**11**)^{10c} were prepared and purified according to literature procedures. Si(*p*-tolyl)₄²¹ was prepared according to the literature procedure and further purified by vacuum sublimation. Si[Si(CH₃)₃]₄ was purchased from Aldrich and used without further purification. (Me₅Cp)₂ZrMe₂,²² Cp₂ZrMe₂,²³ (Me₂Si(Me₄Cp)(*t*-BuN)ZrMe)₂,²⁴ Me₂C(Fluorenyl)(Cp)ZrMe₂,²⁵ Me₂C(Fluorenyl)(Cp)Zr(CH₂Ph)₂,²⁶

(17) Yang, X.; Stern, C. L.; Marks, T. J. *J. Am. Chem. Soc.* **1994**, *116*, 10015.
 (18) Beck, S.; Proscenc, M. H.; Brintzinger, H.-H.; Goretzki, R.; Herfert, N.; Fink, G. *J. Mol. Catal. A: Chem.* **1996**, *111*, 67.
 (19) Chen, M.-C.; Marks, T. J. *J. Am. Chem. Soc.* **2001**, *123*, 11803.

(20) Jia, L.; Yang, X.; Stern, C. L.; Marks, T. J. *Organometallics* **1997**, *16*, 842.
 (21) Lambert, J. B.; Zhao, J.; Stern, C. L.; *J. Phys. Org. Chem.* **1997**, *10*, 229.
 (22) Manriquez, J. M.; McAlister, D. R.; Sanner, R. D.; Bercaw, J. E. *J. Am. Chem. Soc.* **1978**, *100*, 2716.
 (23) Samuel, E.; Rausch, M. D. *J. Am. Chem. Soc.* **1973**, *95*, 6263.
 (24) (a) Stevens, J. C.; Timmers, F. J.; Wilson, D. R.; Schmidt, G. F.; Nickias, P. N.; Rosen, R. K.; Knight, G. W.; Lai, S. Y. (Dow Chemical Co.). Constrained Geometry Addition Polymerization Catalysts, Processes for Their Preparation, Precursors Therefore, Methods of Use, and Novel Polymers Formed Therewith. EP0416815, Mar 13, 1991. (b) Canich, J. M.; Hlatky, G. G.; Turner, H. W. (Exxon Chemical Patents, Inc.). Aluminum-Free Monocyclopentadienyl Metallocene Catalysts for Olefin Polymerization. WO-9200333 A2, Jan 9, 1992. (c) Canich, J. A. M. (Exxon Chemical Patents, Inc.). Olefin Polymerization Catalysts. EP-420436A1, April 3, 1991.
 (25) (a) Razavi, A.; Thewalt, U. *J. Organomet. Chem.* **1993**, *445*, 111. (b) Razavi, A.; Ferrara, J. *J. Organomet. Chem.* **1992**, *435*, 299.
 (26) Bochmann, M.; Lancaster, S. J. *Organometallics* **1989**, *8*, 476.

and $(\text{Me}_5\text{Cp})\text{TiMe}_3^{27}$ were synthesized and purified according to literature procedures. $[(\text{Me}_2\text{SiCp}_2)\text{Zr}(\text{Me})(\text{THF})]^+[\text{MeB}(\text{C}_6\text{F}_5)_3]^-$ (**7**)²⁸ and $[(\text{Me}_2\text{SiCp}_2)\text{Zr}(\text{Me})(\text{PPh}_3)]^+[\text{MeB}(\text{C}_6\text{F}_5)_3]^-$ (**8**)²⁹ were prepared by in situ generation according to literature procedures or by a scale-up reaction followed by purification. Complete resonance assignments for compounds **8**, **9**, and **12** are available in Supporting Information.

$[(\text{Me}_2\text{SiCp}_2)\text{Zr}(\text{Me})(\text{THF})]^+[\text{MeB}(\text{C}_6\text{F}_5)_3]^-$ (7**). Modified Literature Synthesis.** $[(\text{Me}_2\text{SiCp}_2)\text{ZrMe}]^+[\text{MeB}(\text{C}_6\text{F}_5)_3]^-$ (21.4 mg, 26.1 μmol) was loaded into a flip-frit apparatus, which was then interfaced to the high-vacuum line. Dry toluene (approximately 25 mL) was condensed in, under vacuum, in a dry ice/acetone bath, and THF [freshly distilled from Na/K alloy (2.3 μL , 29 μmol)], was added via syringe. The cold bath was next removed and the solution allowed to warm to 25 °C while stirring. The toluene was removed in vacuo. The resultant residue was recooled, and benzene was condensed in. The mixture was warmed to 25 °C and stirred, and the benzene was then removed in vacuo to remove residual toluene. The residue was then triturated overnight in 20 mL of pentane with vigorous stirring and subsequently dried in vacuo. Finally, the solid product was rinsed with benzene (3 \times 2 mL) to remove minor, highly soluble impurities. The final product is very pure by ¹H NMR, and the spectrum is consistent with previous reports.²⁸

In situ Preparation. In the glovebox, $[(\text{Me}_2\text{SiCp}_2)\text{ZrMe}]^+[\text{MeB}(\text{C}_6\text{F}_5)_3]^-$ (11.4 mg, 13.9 μmol) was loaded into a screw-top vial and dissolved in approximately 5 mL of benzene-*d*₆. In a separate glovebox, 9.0 μL (14 μmol) of a THF solution (1.54 M in C₆D₆) was added via gastight syringe. The solution was lightly shaken, and finely dispersed oil was observed. The mixture was loaded into a J-Young NMR tube, and the denser oily phase was allowed to settle to the bottom of the tube. The sample was then used for measurements without further purification.

$[(\text{Me}_2\text{SiCp}_2)\text{Zr}(\text{Me})(\text{PPh}_3)]^+[\text{MeB}(\text{C}_6\text{F}_5)_3]^-$ (8**). In situ Preparation.** In the glovebox, $(\text{Me}_2\text{SiCp}_2)\text{ZrMe}]^+[\text{MeB}(\text{C}_6\text{F}_5)_3]^-$ (16.0 mg, 19.5 μmol) and PPh₃ (5.3 mg, 19.6 μmol) were loaded into a screw-top vial, and approximately 5 mL of benzene-*d*₆ was added. The solution was lightly shaken, and finely dispersed oil was observed. The mixture was loaded into a J-Young NMR tube, and the denser oily phase was allowed to settle to the bottom of the tube. The sample was then used for measurements without further purification. ¹H NMR (C₆D₆, 25 °C): δ 7.07 (m, 9H), 6.93 (m, 6H), 6.64 (pseudo q, 2H), 6.23 (pseudo q, 2H), 5.29 (pseudo q, 2H), 4.89 (pseudo q, 2H), 1.39 (br, 3H), 0.38 (s, 3H), 0.14 (s, 3H), -0.02 (s, 3H). ¹⁹F NMR (C₆D₆, 25 °C): δ -137.07 (brd, ³J_{FF} = 21.0 Hz, 6F, *o*-F), -164.85 (t, ³J_{FF} = 21.4 Hz, 3F, *p*-F), -167.15 (m, 6F, *m*-F).

$[(\text{Me}_2\text{SiCp}_2)\text{Zr}(\text{Me})(\text{THF})]^+[\text{B}(\text{C}_6\text{F}_5)_4]^-$ (9**).** $(\text{Me}_2\text{SiCp}_2)\text{ZrMe}_2$ (50.0 mg, 0.163 mmol) and Ph₃C⁺B(C₆F₅)₄⁻ (71.2 mg, 0.077 mmol) were loaded into a flip-frit apparatus and interfaced to the high-vacuum line. Dry toluene (approximately 25 mL) was condensed in under vacuum in a dry ice/acetone bath. The cold bath was removed and the mixture allowed to warm slowly to 25 °C with stirring. After stirring at 25 °C approximately 30 min, 0.27 mL of a toluene solution of THF was added (0.30 M, 0.081 mmol THF). The toluene was then removed in vacuo. The resulting residue was recooled, and pentane (approximately 25 mL) was condensed in. The mixture was stirred for a few minutes, and the pentane was filtered off to remove unreacted $(\text{Me}_2\text{SiCp}_2)\text{ZrMe}_2$ and Ph₃CCH₃. The solid product was then dried in vacuo (10⁻⁶ Torr). Finally, the solid product was rinsed with benzene (3 \times 2 mL) to remove minor soluble impurities. ¹H NMR (C₆D₆, 25 °C): δ 6.47 (dt, ³J_{HH} = 3.0 Hz, ⁴J_{HH} = 1.8 Hz, 2H), 5.84 (dt, ³J_{HH} = 3.0 Hz, ⁴J_{HH} = 1.8 Hz, 2H), 5.54 (pseudo q, 2H), 5.01 (pseudo q, 2H), 2.83 (m, 4H), 1.13 (m, 4H), 0.32 (s, 3H), 0.23 (s, 3H), -0.07 (s, 3H). ¹⁹F NMR (C₆D₆,

25 °C): δ -137.07 (br, 8F, *o*-F), -164.85 (t, ³J_{FF} = 20.9 Hz, 4F, *p*-F), -166.30 (m, 8F, *m*-F).

$[(\text{Cp}_2\text{Zr})_2(\mu\text{-CH}_2)(\mu\text{-Me})]^+[\text{MePBB}]^-$ (12**).** Compound **12** was generated cleanly in situ by allowing a solution of **11** to stand at 25 °C for 7 days in a J-Young NMR tube. ¹H NMR (C₆D₆, 25 °C): δ 7.51 (s, 2H), 5.89 (s, 20H), -0.83 (br, 3H), -1.49 (s, 3H). ¹⁹F NMR (C₆D₆, 25 °C): δ -123.94 (broad d, 3F), -139.26 (d, ³J_{FF} = 23.7 Hz, 3F), -139.48 (dd, ³J_{FF} = 22.7 Hz, ⁴J_{FF} = 8.9 Hz, 3F), -139.98 (d, ³J_{FF} = 24.1 Hz, 3F), -155.61 (t, ³J_{FF} = 21.3 Hz, 3F), -159.60 (t, ³J_{FF} = 22.7 Hz, 3F), -163.00 (t, ³J_{FF} = 22.0 Hz, 3F), -163.45 (dt, ³J_{FF} = 22.3 Hz, ⁴J_{FF} = 7.2 Hz, 3F), -164.16 (m, 3F).

NOE Measurements. All the NMR experiments were performed using a Bruker Avance DRX 400 equipped with a direct QNP probe and a z -gradient coil controlled by a Great 1/10 gradient unit or a Varian UNITYInova 400 MHz NMR instrument equipped with an inverse probe and a z -gradient coil controlled by a Performa III PFG unit. The ¹H NOESY³⁰ NMR experiments were acquired using the standard three-pulse sequence or by the PFG version as described by Wagner and Berger.³¹ One-dimensional GOESY experiments were carried out as proposed by Shaka and co-workers.³² Two-dimensional ¹⁹F, ¹H HOESY NMR experiments were acquired by using the standard four-pulse sequence or the modified version as proposed by Lix, Sonnichsen, and Syches,³³ in both cases, the fluorine spectra were acquired in the direct dimension. A simple modification of the latter sequence (see Supporting Information) was used to acquire proton-detected one-dimensional ¹H, ¹⁹F HOESY spectra. The shape of the selective pulses was Gaussian, and the duration was 8 ms, while the transmitter power was adjusted to obtain 90° pulses on the fluorine channel. Only a single high-frequency coil for both ¹H and ¹⁹F was used for the measurements carried out with the Varian UNITYInova instrument.³⁴ The number of transients and the number of data points were chosen according to the sample concentration and to the desired final digital resolution. Qualitative or semiquantitative one- or two-dimensional Overhauser spectra were acquired using a 1–2 s relaxation delay and 300–800 ms mixing times. The 2D experiment is preferred in the case of compounds with many resonances in the fluorine spectrum, while 1D ¹H-detected HOESY spectra with selective excitation of ¹⁹F resonances are preferred in the case of low-concentration samples.³⁵ As a control, the two techniques were shown to yield equivalent results in the case of complex **3**.

Quantitative Overhauser experiments for complex **1** were carried out in toluene-*d*₈ at 25 °C. For both the ¹H NOESY and ¹H, ¹⁹F HOESY NMR experiments, a relaxation delay of 25 s and a mixing time of 0.1 s were employed (initial rate approximation).³⁶ Quantitative ¹H NOESY and proton-detected one-dimensional ¹H, ¹⁹F HOESY experiments for complexes **3** and **7** were carried out in benzene-*d*₆ at 25 °C using the pulse sequence shown in Figure S1. A relaxation delay of 6 s and a mixing time of 0.150 s were employed (initial rate approximation).³⁶

PGSE Measurements. All PGSE experiments were performed on the Varian UNITYInova 400 MHz NMR instrument. The standard Stejskal–Tanner pulse sequence, as described by Pregosin and co-

(27) Mena, M.; Royo, P.; Serrano, R.; Pellinghelli, M. A.; Tiripicchio, A. *Organometallics* **1993**, *12*, 633.

(28) Schaper, F.; Geyer, A.; Brintzinger, H.-H. *Organometallics* **2002**, *21*, 473.

(29) Beck, S.; Proscen, M. H.; Brintzinger H.-H. *J. Mol. Catal. A: Chem.* **1998**, *128*, 41.

(30) Jeener, J.; Meier, B. H.; Bachmann, P.; Ernst, R. R. *J. Chem. Phys.* **1979**, *71*, 4546.

(31) Wagner, R.; Berger, S. *J. Magn. Reson. A* **1996**, *123*, 119.

(32) (a) Stott, K.; Stonehouse, J.; Keeler, J.; Hwang, T. L.; Shaka, A. J. *J. Am. Chem. Soc.* **1995**, *117*, 4199. (b) Stonehouse, J.; Adell, P.; Keeler, J.; Shaka, A. J. *J. Am. Chem. Soc.* **1994**, *116*, 6037.

(33) Lix, B.; Sonnichsen, F. D.; Sykes, B. D. *J. Magn. Reson. A* **1996**, *121*, 83.

(34) Urhin, D.; Beatty, E. J.; Barlow, P. N.; Ramage, R.; Sandor, P.; McSparron, H.; Wilken, J.; Starkmann, B.; Young, D. W. *Magn. Moments Online* **1999**, *10*, 1.

(35) The proton-detected 1D experiment is, as expected, more sensitive to subtraction artifacts and sometimes proves to be incompletely efficient in suppressing strong signals not involved in the interactions (e.g., the solvent signal or Si(*p*-tolyl)₄ signals). On the other hand, this represents only a “cosmetic” effect on the final spectrum and does not introduce any difficulties in data interpretation.

(36) Neuhaus, D.; Williamson, M. *The Nuclear Overhauser Effect in Structural and Conformational Analysis*; Wiley-VCH: New York, 2000.

workers, was employed ($\Delta = 54$ ms, $\delta = 3$ ms).³⁷ The nonstimulated version was used because of its greater sensitivity. For this reason, only singlet resonances were usable in the analysis. The gradient pulses were rectangular, and their strength was varied during the course of the experiment. Each spectrum was acquired using 16 K complex points, while the number of transients acquired at each gradient level was adjusted depending on the sample concentration (32 scans at the highest concentrations, 1024 for the lowest concentration). The recycle delay was adjusted for each sample by measuring the T_1 value (using the standard inversion recovery method) for all of the resonances of interest and setting the recycle delay to 5 times the T_1 value of the most slowly relaxing resonance of interest. Signal intensities, I , were measured by integration. Plots of $\ln(I/I_0)$ vs G^2 , according to eq 1, were fitted using a standard linear regression algorithm implemented in the Origin data analysis software package, yielding a slope m (directly proportional to the diffusion coefficient D), with a correlation coefficient consistently greater than 0.999.

$$\ln \frac{I}{I_0} = mG^2 \quad \text{in which} \quad m = (\gamma\delta)^2 D \left(\Delta - \frac{\delta}{3} \right) \quad (1)$$

The diffusion coefficients of four different molecules (standards), namely Si(*p*-tolyl)₄, Si[Si(CH₃)₃]₄, (Me₅Cp)₂ZrMe₂, and Cp₂ZrMe₂, were estimated according to eq 2 by measuring the m parameter for a sample of HDO in D₂O obtained from Aldrich (%D = 99.8).³⁸

$$D_{\text{standard}} = m_{\text{standard}} \frac{D_{\text{HDO}}}{m_{\text{HDO}}} \quad (2)$$

The measurements were carried out on a 10⁻⁴ M benzene-*d*₆ solution of the standards (in this condition it is a reasonable assumption that the solution viscosity can be approximated by that of pure benzene-*d*₆³⁹) at room temperature (~21–23 °C) with the instrument temperature control turned off and without spinning. Due to the temperature dependence of the diffusion coefficient of HDO in D₂O, as well as the temperature dependence of the solvent viscosity, the actual sample temperature inside the probe must be measured. At the beginning and at the end of each PGSE experiment on the standards, both neat methanol and neat ethylene glycol were used to measure the temperature. The actual temperature values were obtained using the standard “tempcal(“m”)” and “tempcal(“e”)” commands implemented in the VNMR 6.1C software package. At 22.0 ± 0.5 °C, the diffusion coefficient of the four compounds were found to be: Si(*p*-tolyl)₄, $D = 8.31 \times 10^{-10}$ m² s⁻¹; Si[Si(CH₃)₃]₄, $D = 1.12 \times 10^{-9}$ m² s⁻¹; (Me₅Cp)₂ZrMe₂, $D = 1.01 \times 10^{-9}$ m² s⁻¹; Cp₂ZrMe₂, $D = 1.22 \times 10^{-9}$ m² s⁻¹.

The diffusion data were treated as recently described by some of us.⁴⁰ According to the Stokes–Einstein model, the diffusion coefficient D can be related to the hydrodynamic radius (r_H) of the diffusing particle according to eq 3:

$$D = \frac{kT}{c\pi\eta r_H} \quad (3)$$

in which k is the Boltzmann constant, T is the absolute temperature, c

is a numerical factor that depends on the size and shape of the solute and the hydrodynamic behavior of the solute–solvent system, and η is the viscosity of the solution. Assuming that both solute and solvent are spherical, the factor c is found to depend on the solute:solvent ratio of radii according to eq 4:⁴¹

$$c = \frac{6}{\left[\frac{3r_{\text{solv}}}{r_H} + \frac{1}{1 + \frac{r_{\text{solv}}}{r_H}} \right]} \quad (4)$$

A semiempirical improvement of eq 4 has been derived:⁴²

$$c = \frac{6}{\left[1 + 0.695 \left(\frac{r_{\text{solv}}}{r_H} \right)^{2.234} \right]} \quad (5)$$

By substituting eq 5 into eq 3, the following expression can be obtained:

$$D = \frac{kT \left[1 + 0.695 \left(\frac{r_{\text{solv}}}{r_H} \right)^{2.234} \right]}{6\pi\eta r_H} \quad (6)$$

It is known from the literature that, for relatively small molecules, the van der Waals radius is the best approximation for the hydrodynamic radius employed in the Stokes–Einstein equation.⁴³ Introducing the van der Waals radius of benzene-*d*₆ (2.7 Å) in eq 6, the hydrodynamic radii of Si(*p*-tolyl)₄, Si[Si(CH₃)₃]₄, (Me₅Cp)₂ZrMe₂, and Cp₂ZrMe₂ were estimated, and the hydrodynamic volumes (V_H) were calculated, pragmatically assuming a spherical shape. Estimation of hydrodynamic volumes for metallocenium ion-pairs by determination of diffusion coefficients could in principle be carried out in the same way, provided that errors originating from variability in gradient strength and temperature could be gauged and that the metallocene concentrations remained low. However, this approach is then not appropriate for concentration-dependent studies. Measurement relative to an internal reference of known diffusion coefficient will reduce errors due to instrument instabilities as well as systematic errors due to changes in solution viscosity.⁴⁴ In principle, any internal reference with a molecular volume similar to that of the species under investigation could be used. We chose Si(*p*-tolyl)₄ as an internal standard which combines high chemical inertness toward metallocenium ion-pair complexes and a suitable NMR spectrum with a sharp singlet at δ 2.10 ppm in benzene-*d*₆ that does not overlap with the resonances of the species under investigation.

Samples were prepared in the glovebox using a 10⁻³ M stock solution of Si(*p*-tolyl)₄ in benzene-*d*₆. The samples were then transferred into a PTFE-valved J-Young NMR tube and kept frozen at -78 °C before use. The actual concentration of each sample was determined by integration versus the Si(*p*-tolyl)₄ internal standard. Variation of the sample concentrations was achieved by diluting the most concentrated sample with the same 10⁻³ M stock solution of Si(*p*-tolyl)₄ in benzene-*d*₆. In some cases, to reduce total experiment time, additional Si(*p*-tolyl)₄ was added to a given NMR sample. For each experiment, the diffusion coefficient value obtained for a given compound at a given concentration was corrected using the internal standard. In this way,

(37) (a) Valentini, M.; Rügger, H.; Pregosin, P. S. *Helv. Chim. Acta* **2001**, *84*, 2833. (b) Valentini, M.; Pregosin, P. S.; Rügger, H. *Organometallics* **2000**, *19*, 2551. (c) Holz, M.; Weingärtner, H. *J. Magn. Reson.* **1991**, *92*, 115.

(38) Mills, R. *J. Phys. Chem.* **1973**, *77*, 685. Data at different temperatures were estimated by interpolation of the data reported by Mills, giving $D_{\text{HDO}} = 1.748 \times 10^{-9}$ m² s⁻¹ at 22 °C.

(39) Viscosity of C₆D₆ was estimated to be 0.672 cp at 22 °C by interpolation of the data reported for C₆H₆ (*CRC Handbook of Chemistry and Physics*, 51st ed.; Weast, R. C., Ed.; Chemical Rubber: Cleveland, 1971 and *CRC Handbook of Chemistry and Physics*, 77th ed.; Lide, D. R., Ed.; CRC Press: New York, 1996) and application of the correction proposed by Mills (Mills, R. *J. Phys. Chem.* **1976**, *80*, 888): $\eta(\text{C}_6\text{D}_6) = 1.063 \times \eta(\text{C}_6\text{H}_6)$.

(40) Zuccaccia, D.; Sabatini, S.; Bellachioma, G.; Cardaci, G.; Clot, E.; Macchioni, A. *Inorg. Chem.* **2003**, *42*, 5465.

(41) (a) Espinosa, P. J.; de la Torre, J. G. *J. Phys. Chem.* **1987**, *91*, 3612. (b) Gierer, A.; Wirtz, K. *Z. Naturforsch. A* **1953**, *8*, 522. (c) Wirtz, K. *Z. Naturforsch. A* **1953**, *8*, 532.

(42) Chen, H.-C.; Chen, H.-S. *J. Phys. Chem.* **1984**, *88*, 5118.

(43) Edward, J. T. *J. Chem. Educ.* **1970**, *47*, 261.

(44) See for example: (a) Macchioni, A.; Romani, A.; Zuccaccia, C.; Guglielmetti G.; Querci C. *Organometallics* **2003**, *22*, 1526. (b) Babushkin, D. E.; Brintzinger, H.-H. *J. Am. Chem. Soc.* **2002**, *124*, 12869. (c) Burini, A.; Fackler, J. P. Jr.; Galassi, R.; Macchioni, A.; Omary, M. A.; Rawashdeh-Omary, M. A.; Pietroni, B. R.; Sabatini, S.; Zuccaccia, C. *J. Am. Chem. Soc.* **2002**, *124*, 4570. (d) Zuccaccia, C.; Bellachioma, G.; Cardaci G.; Macchioni A. *Organometallics* **2000**, *19*, 4663.

Table 1. Diffusion Coefficients (D , 10^{-10} m² s⁻¹), Corrected Diffusion Coefficients^a (D^* , 10^{-10} m² s⁻¹), Hydrodynamic Radii (r_H , Å), Hydrodynamic Volumes (V_H , Å³), c Factor, and Aggregation Number (N) Values at Various Concentrations (units 10^{-3} M) for the Standards, the Neutral Metallocenium Precursors, and the ISIPs^b

	concn	D	D_{TPTS}	D^*	r_H	c	V_H	N
Si(<i>p</i> -tolyl) ₄ (TPTS)	0.10	8.31 ^c			4.66	5.0	424	1.20
Si[Si(CH ₃) ₃] ₄ (TMSS)	0.10	11.2 ^c			3.80	4.5	232	0.86
(Me ₅ Cp) ₂ ZrMe ₂	0.10	10.1 ^c			4.06	4.7	280	0.86
Cp ₂ ZrMe ₂	0.10	12.2 ^c			3.63	4.4	200	1.11
(Me ₅ Cp)TiMe ₃	9.75	11.8	8.20	12.0	3.64	4.4	202	0.95
Me ₂ C(Fluorenyl)(Cp)ZrMe ₂	2.46	9.44	7.94	9.89	4.13	4.7	295	1.01
Me ₂ Si(Me ₄ Cp)(<i>t</i> -BuN)ZrMe ₂	8.74	9.92	7.77	10.6	3.94	4.6	256	0.86
Me ₂ C(Fluorenyl)(Cp)Zr(CH ₂ Ph) ₂	2.00	7.69	7.77	8.23	4.70	5.0	435	0.96
(Me ₅ Cp) ₂ ZrMe ₂	7.34	9.63	8.02	9.97	4.11	4.7	291	0.89
Cp ₂ ZrMe ₂	15.67	11.1	7.11	12.9	3.47	4.3	175	0.97
[Me ₂ Si(Me ₄ Cp)(<i>t</i> -BuN)TiMe] ⁺ [MeB(C ₆ F ₅) ₃] ⁻	9.90	6.86	7.79	7.32	5.12	5.1	562	0.99
[Me ₂ C(Fluorenyl)(Cp)ZrMe] ⁺ [MeB(C ₆ F ₅) ₃] ⁻	4.80	6.64	7.66	7.20	5.19	5.2	586	1.03
[(Me ₅ Cp) ₂ ThMe] ⁺ [B(C ₆ F ₅) ₄] ⁻ (6)	0.80	6.62	8.02	6.85	5.39	5.2	656	0.96
[Cp ₂ ZrMe] ⁺ [MeB(C ₆ F ₅) ₃] ⁻ (1)	2.50	7.08	7.63	7.71	4.92	5.1	499	1.11
[(Me ₂ Cp) ₂ ZrMe] ⁺ [MeB(C ₆ F ₅) ₃] ⁻ (2)	5.00	6.92	7.61	7.56	5.00	5.1	524	1.03
	1.00	6.72	7.40	7.56	5.00	5.1	524	1.03
[(Me ₂ SiCp) ₂ ZrMe] ⁺ [MeB(C ₆ F ₅) ₃] ⁻ (3)	8.60	6.53	7.27	7.46	5.05	5.1	539	1.01
	2.80	6.55	7.21	7.55	5.00	5.1	524	0.98
	1.37	6.58	7.24	7.56	5.00	5.1	524	0.98
	0.68	6.81	7.42	7.63	4.97	5.1	514	0.97
[Me ₂ C(Fluorenyl)(Cp)ZrMe] ⁺ [FPBA] ⁻ (4)	5.00	5.34	7.03	6.31	5.76	5.3	800	0.99
	2.80	5.76	7.54	6.35	5.72	5.3	784	0.97
	1.15	6.20	8.08	6.38	5.70	5.3	776	0.96
[C ₂ H ₄ (Indenyl) ₂ ZrMe] ⁺ [FPBA] ⁻ (5)	3.50	6.00	7.82	6.37	5.70	5.3	776	0.96
	2.05	5.40	7.07	6.35	5.72	5.3	784	0.97

^a The corrected D^* values correspond to a hypothetical measurement carried out at 22 °C, in a solution containing the reported nominal concentration, but having the viscosity of pure C₆D₆ (see Experimental Section for details). ^b The numbers in bold are represented graphically in Figure 1. ^c Carried out at 22 °C.

the corrected values correspond to a hypothetical experiment carried out at 22.0 ± 0.5 °C in which the solution viscosity is approximated by the bulk solvent viscosity. Hydrodynamic radii (r_H) were obtained by application of eq 6, and hydrodynamic volumes (V_H) were calculated assuming a spherical shape. Data are reported in terms of the ratio of the apparent PGSE experimental volume at a given concentration to the van der Waals volume of the 1:1 ion-pair calculated from X-ray coordinates or molecular modeling. This ratio represents the aggregation number (N) in a way similar to that defined by Pochapsky⁴⁵ and is useful when trends over a range of concentrations are to be compared. Structural models for cations and anions were obtained from experimental crystal structure data (Cambridge Structural Database) or by a simple energy minimization using the Spartan software package when a crystal structure was not available. In the case of the outer sphere ion-pairs, the two ions were modeled separately. These models were then used to estimate the van der Waals volumes using the software package WebLab Viewer.

The measurement uncertainty in the diffusion data was estimated by determining the standard deviation of the ratio $m_{\text{species}}/m_{\text{standard}}$ for a benzene-*d*₆ solution containing 2.8×10^{-3} M of [(Me₂SiCp)₂ZrMe]⁺[MeB(C₆F₅)₃]⁻ (**3**) and 1×10^{-3} M of Si(*p*-tolyl)₄ across the series $\Delta = 34, 54, 74,$ and 94 ms.³⁷ Standard propagation of errors analysis yielded a standard deviation of approximately 1.7% in the radius and thus 5% in the volume. Any remaining deviations of the PGSE-derived volumes from the computed van der Waals volumes of the ISIPs are most likely due to deficiencies in the modified Stokes–Einstein model and in the assumption that hard-sphere van der Waals volumes are a good representation of the hydrodynamic volume of a given species. Representative examples of the PGSE data acquisitions are reported in the Supporting Information.

X-ray Crystal Structure Determination of [(Me₂SiCp)₂Zr(Me)-(THF)]⁺[B(C₆F₅)₄]⁻ (9**).** Crystals of **9** suitable for X-ray diffraction were obtained as colorless needles by heating an NMR tube containing

an excess of solid **9** and benzene-*d*₆ to reflux and allowing it to stand at room temperature for 3 h. A crystal of dimensions 0.540 mm × 0.150 mm × 0.100 mm was selected and mounted under Infineum V8512 oil and held under a nitrogen cold-stream at 153(2) K for data collection. Diffraction data were obtained using a Bruker SMART 1000 CCD area detector diffractometer with a fine-focus, sealed tube Mo K α radiation source ($\lambda = 0.71073$ Å), and graphite monochromator: space group $P2_1/c$, $Z = 4$, $a = 16.037(3)$ Å, $b = 16.263(3)$ Å, $c = 18.351(3)$ Å, $\beta = 104.515(3)^\circ$, $V = 4633.2(14)$ Å³, $D_{\text{calc}} = 1.608$ g/cm³, $F(000) = 2240$. Of 37809 measured reflections, 10806 were independent and 6273 gave $I > 2\sigma(I)$. The initial crystal structure solution was obtained by direct methods and refined through successive least-squares cycles, and a face-indexed absorption correction was applied: $\mu = 0.381$ mm⁻¹, $T_{\text{min}} = 0.87164$, $T_{\text{max}} = 0.96566$. The refinement was carried to convergence. Hydrogen atoms were placed in idealized positions and refined isotropically with fixed U_{eq} under standard riding model constraints: $(\Delta/\sigma)_{\text{max}} = 0.022$, $(\Delta/\sigma)_{\text{mean}} = 0.001$, $\Delta\rho_{\text{max}} = 1.488$ e/Å³ (adjacent to Zr), $\Delta\rho_{\text{min}} = -0.734$ e/Å³, $R[F^2 > 2\sigma(F^2)] = 5.92\%$, $wR(F^2) = 15.84\%$. Full crystal data collection and refinement parameters can be found in the Crystallographic Information File.

Results

PGSE and NOE NMR Investigations of Inner Sphere Ion-Pairs (ISIPs). Table 1 summarizes the results of the PGSE measurements carried out on inner sphere metallocenium ion-pairs and on some neutral alkylmetallocenes with various ligand frameworks. Hydrodynamic volumes are graphically depicted in Figure 1 in comparison with the crystallographically or computationally derived van der Waals volumes. There is very good agreement between the experimental hydrodynamic volumes and the van der Waals volumes, which indicates that all of these complexes exist in solution predominantly, if not exclusively, as discrete 1:1 ion-pairs. As far as the ISIPs are concerned, concentration-dependent PGSE measurements were performed on compounds **2**, **3**, **4**, and **5**. All show invariant

(45) (a) Mo, H.; Pochapsky, C. T. *J. Phys. Chem. B.* **1997**, *101*, 4485. (b) Pochapsky, S. S.; Mo, H.; Pochapsky, C. T. *J. Chem. Soc., Chem. Commun.* **1995**, 2513.

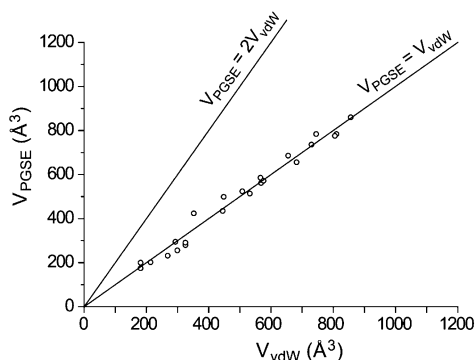


Figure 1. Plot of PGSE-derived hydrodynamic volumes (V_{PGSE}) versus van der Waals volumes (V_{vdW}) computed for various metallocenium compounds. The data points refer to the values reported in bold in Tables 1 and 5.

apparent molecular volumes over a wide range of concentrations. Compound **3**, for example, continues to behave as a single 1:1 ion-pair up to 8.0 mM.⁴⁶

The ^1H , ^{19}F HOESY spectrum of complex **1** evidences strong NOE interactions between the *o*-F nuclei of the $\text{B}(\text{C}_6\text{F}_5)_3$ moiety and the μ -Me group as well as between $\text{B}(\text{C}_6\text{F}_5)_3$ *o*-F nuclei and protons on the Zr-Me group and Cp ligands (Cp = cyclopentadienyl). No cation–anion NOE interactions are observed for the $\text{B}(\text{C}_6\text{F}_5)_3$ *m*-F and *p*-F fluorine nuclei. In complex **3** the *ansa*- Me_2Si bridge inhibits free rotation of the Cp ligands, allowing determination of the relative orientation of the anion with respect to the cation. The ^1H , ^{19}F HOESY spectrum of complex **3** is shown in Figure 2, and a section of the corresponding ^1H NOESY spectrum is shown in Figure 3. The intensity of the interactions between the *o*-F fluorine nuclei on the anion and the Cp protons in the ^1H , ^{19}F HOESY spectrum follows the order $\text{H2} > \text{H1} > \text{H3}$, and no cross-peaks are detectable for the H4 proton. This indicates that the preferred contact point for the anion is proximate to H2 (Figure 2). This contention is confirmed by the strong homonuclear cross-peak between the μ -Me group and the H2 proton in the ^1H NOESY spectrum (Figure 3). As in the case of complex **1**, no ^{19}F – ^1H interionic interactions are detected for the *m*-F and *p*-F nuclei.

Complex **5** exists in solution as a 69:31 mixture of diastereomers as a consequence of the chirality in both the $[\text{FPBA}]^-$ anion and in the cation. This observation alone suggests that this complex is present in solution mainly as a tight ion-pair. Several interionic proton–fluorine dipolar interactions can be detected in the corresponding ^1H , ^{19}F HOESY spectrum (Figure 4).⁴⁷ The Al–F, F6, F5, and *o*-F* fluorine atoms interact with the protons on the cation, and in particular, for the major diastereomer, the following contacts can be detected: Al–F with H2, Zr-Me, H13, and H12/H3; F6 with H2, H1, Zr-Me, and

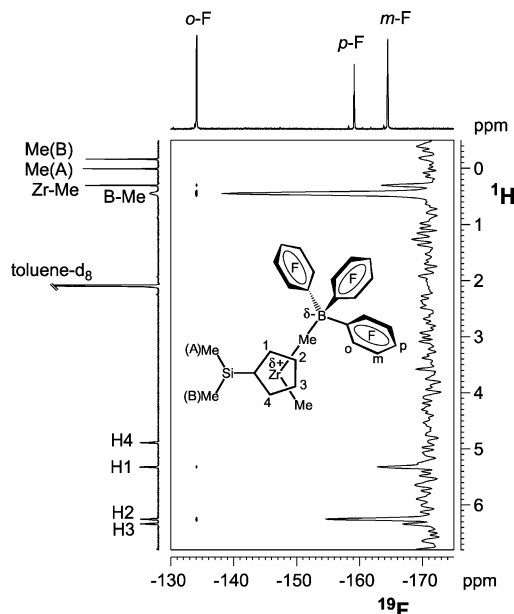


Figure 2. Section of the ^{19}F , ^1H HOESY spectrum (376.4 MHz, relaxation delay = 2 s, mixing time = 800 ms, toluene- d_8 , 298 K) of complex **3**. The F1 trace (indirect dimension) relative to the *o*-F resonance is reported on the right. See Figure S7 for the corresponding proton-detected one-dimensional ^1H , ^{19}F HOESY experiments.

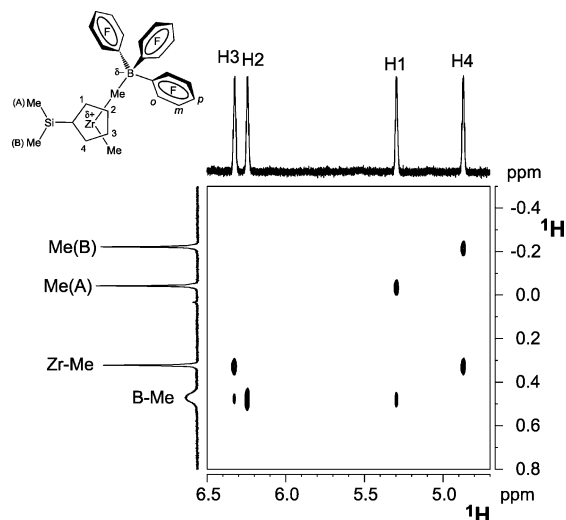


Figure 3. Section of the ^1H NOESY spectrum (399.94 MHz, relaxation delay = 6 s, mixing time = 150 ms, benzene- d_6 , 298 K) of complex **3**.

H12/H3; F5 with H3/H12, H10, and H11; and *o*-F* with H2, H11, H1, and H12/H3. The ^{19}F , ^1H HOESY spectrum of compound **6** (see Supporting Information) shows that both the *o*-F and *m*-F fluorine atoms of the $[\text{B}(\text{C}_6\text{F}_5)_4]^-$ anion exhibit NOE interactions with both the Cp-Me and the Th-Me protons. A very small interaction is also observed between the Cp-Me group and the *p*-F nuclei.

The possibility of estimating the average internuclear distances in solution was also explored by acquiring quantitative homo- and heteronuclear NOE spectra using the initial rate approximation.³⁶ The average interionic internuclear distances derived for complexes **1** and **3** are compared in Tables 2 and 3.

PGSE and NOE NMR Investigations of Outer Sphere Ion-Pairs (OSIPs). Upon addition of 1.0 equiv of THF or PPh_3 to complex **3**, the methylborate anion is displaced from the metal center to form OSIPs **7** and **8**, respectively.^{28,29} The ^1H NOESY

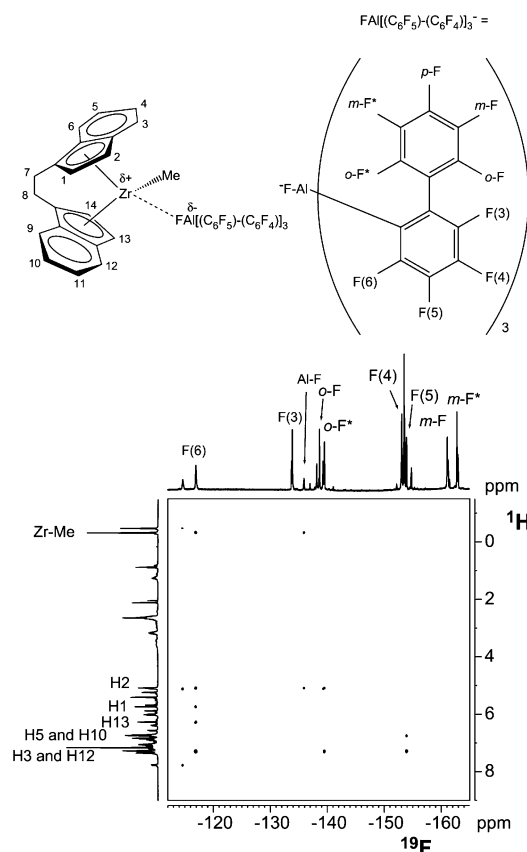
(46) By dissolving purified complex **3** (see ref 16) at room temperature in benzene- d_6 , the highest concentration we were able to achieve was 2.8 mM. The 8.6 mM solution was obtained by heating the NMR tube at the reflux temperature of the solvent while some solid was still present on the bottom of the tube; the initial NMR spectrum shows little evidence of decomposition. According to the data of Brintzinger and co-workers (Beck S.; Lieber, S.; Schaper, F.; Geyer, A.; Brintzinger, H.-H. *J. Am. Chem. Soc.* **2001**, *123*, 1483), this same compound, formed in situ from the corresponding dimethyl complex with a slight excess (1.1 equiv) of $\text{B}(\text{C}_6\text{F}_5)_3$, could be maintained in C_6D_6 solution at a concentration around 20 mM.

(47) The assignments of both ^1H and ^{19}F resonances were made using homonuclear COSY and NOESY experiments (see Supporting Information). Due to the extensive spectral overlap in the ^1H spectrum of the major isomer, the proton resonances were assigned using the more resolved resonances of the minor isomer, taking advantage of the selective EXSY peaks due to the rapid anion racemization (see ref 10c).

Table 2. Comparison between Experimental and Theoretical Average Internuclear Distances (Å) for Complex 1

	calculated ^a	experimental ^b		calculated ^c	experimental ^c
$\langle r \rangle_{\text{Zr-Me/Cp}} / \langle r \rangle_{\text{B-Me/Cp}}$	1.00	0.99	$\langle r \rangle_{\text{B-Me/Cp}}$	3.8	3.8
$\langle r \rangle_{\text{o-F/B-Me}} / \langle r \rangle_{\text{o-F/Zr-Me}}$	0.69	0.69	$\langle r \rangle_{\text{o-F/Zr-Me}}$	4.8	4.8
$\langle r \rangle_{\text{o-F/B-Me}} / \langle r \rangle_{\text{o-F/Cp}}$	0.64	0.73	$\langle r \rangle_{\text{o-F/Cp}}$	5.2	4.6
	0.81 ^d			4.1 ^d	

^a Calculated from X-ray metrical parameters,⁴⁹ considering all possible internuclear vectors, assuming that rotation of the methyl groups is faster than the overall molecular correlation time (r^{-3} average).⁷⁵ ^b Calculated from the relative cross-peak integrals, taking into account the number of equivalent nuclei.⁷⁶ ^c In the case of H–H distances, the reference distance is $\langle r \rangle_{\text{Zr-Me/Cp}}$ (3.8 Å), while in the case of F–H, the reference distance is $\langle r \rangle_{\text{o-F/BMe}}$ (3.4 Å). Both are calculated from the X-ray structure,⁴⁹ considering all the possible internuclear vectors and assuming that the rotation of the methyl groups is more rapid than the overall molecular correlation time (r^{-3} average). ^d Calculated from X-ray metrical parameters,⁴⁹ considering all possible internuclear vectors and assuming that rotation of the interionic average vector connecting the Cp protons and the *o*-F fluorine atoms is slower than the overall ion-pair correlation time (r^{-6} average). In this case, it is likely that the difference between the internal motion and the overall relaxation time is less pronounced, so that neither model reproduces the experimental data well.

**Figure 4.** ¹⁹F,¹H HOESY spectrum (376.6 MHz, relaxation delay = 1 s, mixing time = 800 ms, benzene-*d*₆, 298 K) of complex 5.

spectrum of a 1.7 mM solution of **7** in benzene-*d*₆ is illustrated in Figure 5. Homonuclear interionic NOE interactions are observed between the B-Me group and the H1 protons of the [(Me₂SiCp₂)Zr(Me)(THF)]⁺ cation. In addition, the interactions of both the α and β THF protons and the Cp protons with the *o*-F (medium) and *m*-F (medium-weak) nuclei of the MeB(C₆F₅)₃⁻ counteranion are clearly visible in the 1D ¹H,¹⁹F HOESY spectrum (Figure 6). The interaction intensities for the Cp protons follow the order H1 > H2 ≫ H3 and, in contrast to complex **3**, the strongest contact is no longer with H2 but with H1.

The 1D ¹H,¹⁹F HOESY spectrum of a 1.1 mM benzene-*d*₆ solution of complex **8** reveals the same interionic interactions with almost the same intensity trends as observed for **7** above (Figure 7). Increasing the concentration of **8** leads to a loss of specificity in anion–cation interactions; the 1D ¹H,¹⁹F HOESY spectrum of a 2.4 mM solution of **8** shows that all of the cation

Table 3. NOESY- and HOESY-Derived Internuclear Distances (Å) for Complex 3

	experimental		experimental
$\langle r \rangle_{\text{o-F/B-Me}}$	3.4 ^a	$\langle r \rangle_{\text{Zr-Me/H3}}$	3.1 ^a
$\langle r \rangle_{\text{o-F/H2}}$	4.1 ^b	$\langle r \rangle_{\text{Me(A)/H1}}$	3.2 ^b
$\langle r \rangle_{\text{o-F/H1}}$	4.7 ^b	$\langle r \rangle_{\text{Me(B)/H4}}$	3.2 ^b
$\langle r \rangle_{\text{o-F/H3}}$	5.1 ^b	$\langle r \rangle_{\text{Zr-Me/H4}}$	3.2 ^b
$\langle r \rangle_{\text{o-F/Me-Zr}}$	5.0 ^b	$\langle r \rangle_{\text{B-Me/H2}}$	3.0 ^b
		$\langle r \rangle_{\text{B-Me/H1}}$	3.7 ^b
		$\langle r \rangle_{\text{B-Me/H3}}$	3.9 ^b

^a Calculated from X-ray metrical parameters of complex **1**, considering all possible internuclear vectors and assuming that rotation of the methyl groups is faster than the overall molecular correlation time (r^{-3} average).⁷⁵ ^b Calculated from the relative cross-peak integrals, taking into account the number of equivalent nuclei,⁷⁶ using the $\langle r \rangle_{\text{o-F/B-Me}}$ (3.4 Å) as a reference distance for the H–F distances, and the $\langle r \rangle_{\text{Zr-Me/H3}}$ (3.1 Å) for the H–H distances.

Table 4. NOESY- and HOESY-derived Interionic Heteronuclear Distances (Å) for Complex 7

	experimental		experimental	calculated ^a
$\langle r \rangle_{\text{o-F/B-Me}}$	3.4 ^a	$\langle r \rangle_{\text{Zr-Me/H3}}$	3.1 ^a	3.1
$\langle r \rangle_{\text{o-F/H2}}$	4.6 ^b	$\langle r \rangle_{\text{Me(A)/H1}}$	3.3 ^b	3.3
$\langle r \rangle_{\text{o-F/H1}}$	4.5 ^b	$\langle r \rangle_{\text{Me(B)/H4}}$	3.4 ^b	3.4
$\langle r \rangle_{\text{o-F/H3}}$	5.1 ^b	$\langle r \rangle_{\text{Zr-Me/H4}}$	3.2 ^b	3.2
$\langle r \rangle_{\text{o-F}/\alpha}$	4.9 ^b	$\langle r \rangle_{\text{Zr-Me}/\alpha}$	3.7 ^b	4.0
$\langle r \rangle_{\text{o-F}/\beta}$	5.1 ^b	$\langle r \rangle_{\text{B-Me/H1}}$	4.1 ^b	4.1
		$\langle r \rangle_{\beta/\text{H2}}$	4.5 ^b	4.6
		$\langle r \rangle_{\alpha/\text{H1}}$	3.7 ^b	4.1
		$\langle r \rangle_{\alpha/\text{H2}}$	3.2 ^b	3.2
		$\langle r \rangle_{\alpha/\text{H3}}$	3.9 ^b	4.4

^a Calculated from X-ray metrical parameters of the cationic portion of complex **9**, considering all possible internuclear vectors and assuming that rotation of the methyl groups is faster than the overall molecular correlation time (r^{-3} average).⁷⁵ ^b Calculated from the relative cross-peak integrals, taking into account the number of equivalent nuclei,⁷⁶ using the $\langle r \rangle_{\text{o-F/B-Me}}$ (3.4 Å) as a reference distance for the H–F distances, and the $\langle r \rangle_{\text{Zr-Me/H3}}$ (3.1 Å) for the H–H distances.

Cp and PPh₃ protons interact with the anion *o*-F and *m*-F nuclei (Figures 7 and S3). In contrast, the specificity of interionic interactions in **7** appears unaffected or affected to a lesser extent by increased concentration (Figure 6). The average interionic internuclear distances measured for complex **7** are summarized in Table 4.

The apparent PGSE-derived volumes of complexes **7** and **8** exhibit dramatic concentration dependence. The results are reported in Table 5 and graphically depicted in Figure 8a. It can be seen that with increasing concentration, both **7** and **8** exhibit similar tendencies to form ion-quadruples or even higher aggregates in the case of **8**, with the principal difference being that **8**, probably due to the presence of an increased number of phenyl substituents, can be maintained at higher concentrations in benzene-*d*₆.

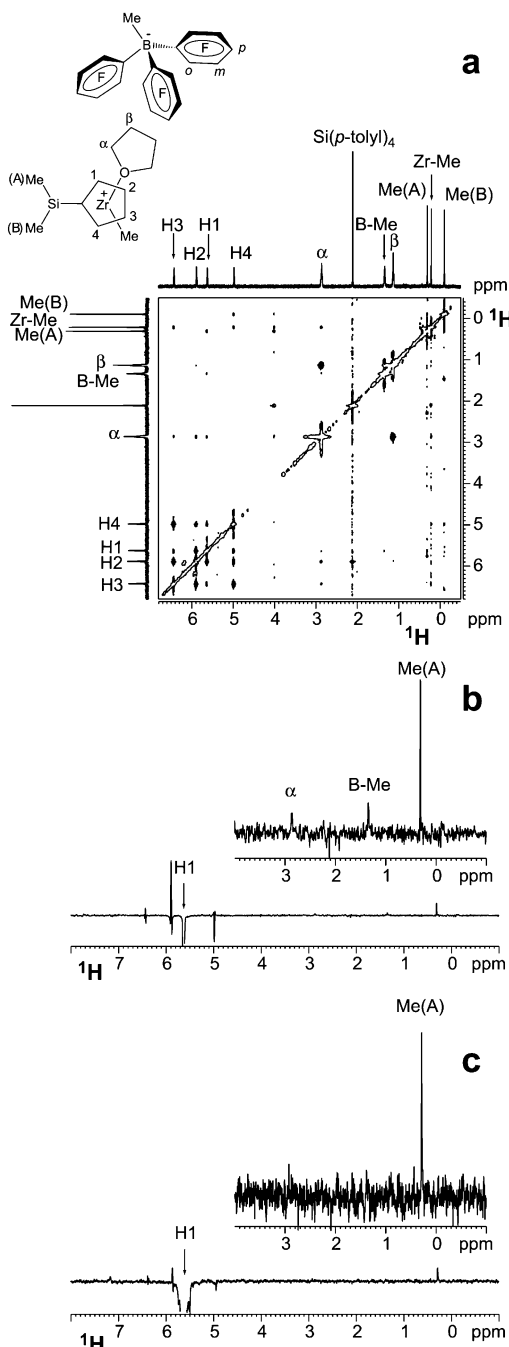


Figure 5. (a) Section of the ^1H NOESY spectrum (399.94 MHz, relaxation delay = 6 s, mixing time = 150 ms, benzene- d_6 , 298 K) of a 1.7 mM solution of complex **7**. As evident from the F2 traces, the apparent H1/H3 and H2/H4 cross-peaks are dispersion peaks due to subtraction imperfections. (b) F2 trace (direct dimension) corresponding to the H1 resonance of the 2D spectrum. (c) 1D-GOESY experiment (H1 irradiation, relaxation delay = 6 s, mixing time = 150 ms, benzene- d_6 , 298 K) of a ca. 0.6 mM solution of complex **7**.

Compound **9** has very low solubility in benzene- d_6 at room temperature. Its apparent volume (Figure 8b) in a saturated solution (ca. 0.4 mM) is consistent with the presence of 1:1 ion-pairs. There is no evidence for aggregate formation. Higher concentrations can be reached by heating the NMR tube containing solid **9** and benzene- d_6 to 60 °C. After approximately 30 min at 25 °C, complex **9** begins to separate from this supersaturated solution as crystals. Even if a quantitative PGSE investigation cannot be carried out under these conditions, a

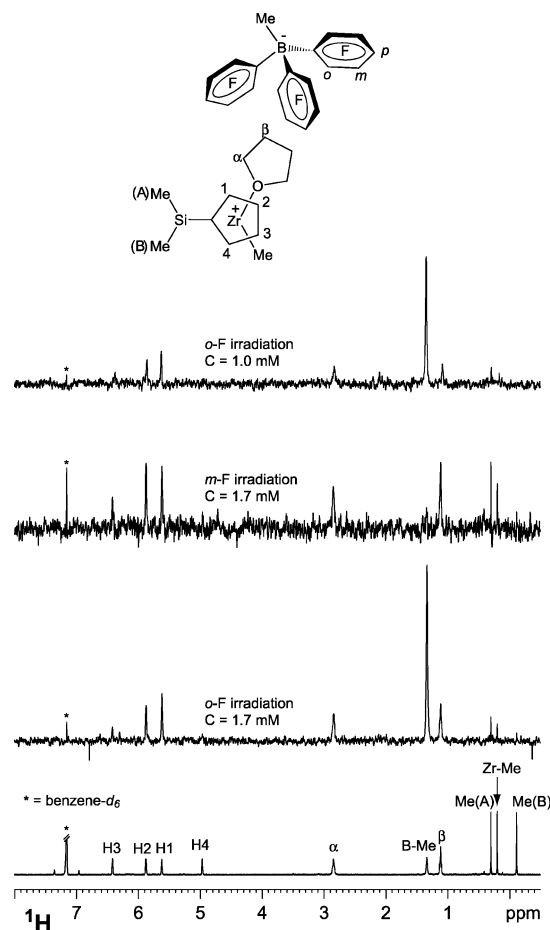


Figure 6. Proton (bottom) and 1D ^1H , ^{19}F HOESY spectra (middle: *o*-F and *m*-F irradiations; top: *o*-F irradiation, 1.0 mM) of complex **7** (399.94 MHz, relaxation delay = 2 s, mixing time = 800 ms, 1.7 mM in benzene- d_6 , 298 K).

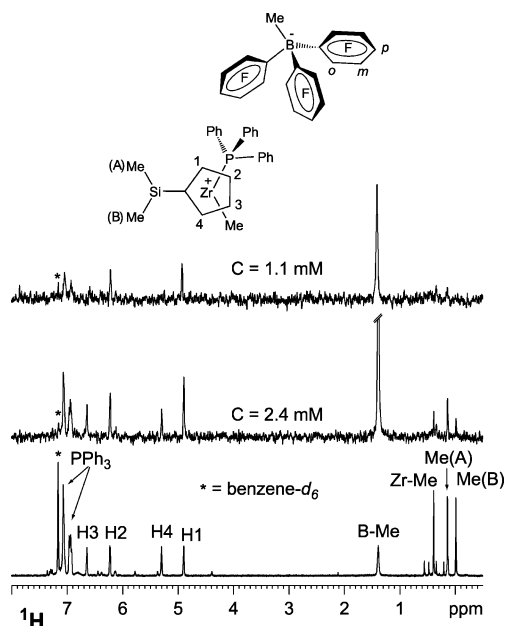


Figure 7. Proton (bottom) and 1D ^1H , ^{19}F HOESY spectra (middle: *o*-F irradiation; top: *o*-F irradiation, 1.1 mM) of compound **8** (399.94 MHz, relaxation delay = 2 s, mixing time = 800 ms, 2.4 mM in benzene- d_6 , 298 K).

quickly executed experiment indicates the formation of aggregates (N = apparent aggregation number = 1.7 at 1.5 mM).

Table 5. Diffusion Coefficients (D , 10^{-10} m 2 s $^{-1}$), Corrected Diffusion Coefficients^a (D^* , 10^{-10} m 2 s $^{-1}$), Hydrodynamic Radii (r_H , Å), Hydrodynamic Volumes (V_H , Å 3), Factor c , and Aggregation Number (N) Values at Different Concentrations (Concentration, 10^{-3} M) for the OSIP^a

	concn	D	D_{PTS}	D^*	r_H	c	V_H	N
[(Me $_2$ SiCp) $_2$ Zr(Me)(THF)] $^+$ [MeB(C $_6$ F $_5$) $_3$] $^-$ (7)	2.20	5.17	7.45	5.76	6.19	5.4	993	1.72
	1.70	5.76	7.98	6.00	5.99	5.4	900	1.56
	1.60	4.87	6.67	6.07	5.94	5.4	878	1.52
	1.20	5.76	7.55	6.34	5.73	5.3	788	1.37
	0.99	6.01	7.59	6.57	5.57	5.3	724	1.26
	0.90	5.93	7.42	6.65	5.52	5.3	705	1.22
	0.70	6.20	7.36	7.00	5.30	5.2	624	1.08
	0.09	6.74	7.71	7.27	5.15	5.2	572	0.99
	3.10	4.11	7.20	4.74	7.30	5.6	1630	2.19
[(Me $_2$ SiCp) $_2$ Zr(Me)(PPh $_3$)] $^+$ [MeB(C $_6$ F $_5$) $_3$] $^-$ (8)	2.35	4.29	7.21	4.95	7.03	5.5	1455	1.95
	1.40	4.93	7.53	5.44	6.50	5.5	1150	1.54
	1.05	5.06	7.44	5.66	6.29	5.4	1042	1.40
	0.91	4.96	7.18	5.73	6.22	5.4	1008	1.35
	0.86	5.36	7.67	5.81	6.15	5.4	974	1.31
	0.45	5.80	7.50	6.43	5.67	5.3	764	1.02
	0.12	5.85	7.65	6.36	5.72	5.3	784	1.05
	1.48	5.15	7.74	5.53	6.40	5.5	1098	1.68
	0.82	5.88	7.70	6.34	5.73	5.3	788	1.20
[(Me $_2$ SiCp) $_2$ Zr(Me)(THF)] $^+$ [B(C $_6$ F $_5$) $_4$] $^-$ (9)	0.38	6.37	7.86	6.73	5.47	5.2	686	1.05
	0.64	5.04	7.20	5.81	6.15	5.4	974	1.33
	0.42	5.38	7.19	6.22	5.82	5.3	826	1.13
[Me $_2$ Si(Me $_4$ Cp)(<i>t</i> -BuN)Zr(Me)(C $_6$ D $_6$)] $^+$ [B(C $_6$ F $_5$) $_4$] $^-$ (10)	0.24	5.64	7.28	6.43	5.66	5.3	760	1.04
	0.12	5.73	7.30	6.53	5.60	5.3	736	1.01
	5.20	4.50	7.35	5.09	6.87	5.5	1358	1.59
[Cp $_2$ ZrMe) $_2$ (μ -Me)] $^+$ [MePBB] $^-$ (11)	3.30	4.22	6.79	5.17	6.78	5.5	1306	1.53
	2.00	4.58	7.00	5.44	6.49	5.5	1145	1.34
	0.97	4.85	7.00	5.76	6.19	5.4	993	1.16
	0.55	5.02	7.06	5.91	6.07	5.4	937	1.09
	0.11	5.15	7.01	6.11	5.90	5.4	860	1.01

^a The numbers in bold are represented graphically in Figure 1. ^a The corrected D^* value correspond to a hypothetical measurement carried out at 22 °C, in a solution containing the reported nominal concentration, but having the viscosity of pure C $_6$ D $_6$ (see Experimental Section for details).

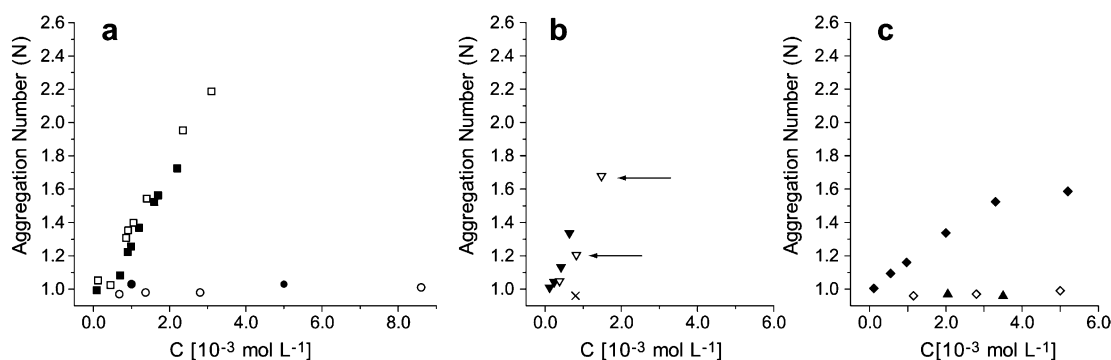


Figure 8. PGSE-derived aggregation number (N) as a function of concentration for inner- and outer-sphere metalocenium complexes. The two arrows in frame b indicate measurements that refer to a supersaturated solution. □ [(Me $_2$ SiCp) $_2$ Zr(Me)(PPh $_3$)] $^+$ [MeB(C $_6$ F $_5$) $_3$] $^-$ (**8**); ■ [(Me $_2$ SiCp) $_2$ Zr(Me)(THF)] $^+$ [MeB(C $_6$ F $_5$) $_3$] $^-$ (**7**); ● [(1,2-Me $_2$ Cp) $_2$ ZrMe] $^+$ [MeB(C $_6$ F $_5$) $_3$] $^-$ (**2**); ○ [(Me $_2$ SiCp) $_2$ ZrMe] $^+$ [MeB(C $_6$ F $_5$) $_3$] $^-$ (**3**); ▼ [(Me $_2$ Si(Me $_4$ Cp)(*t*-BuN)Zr(Me)(benzene- d_6)] $^+$ [B(C $_6$ F $_5$) $_4$] $^-$ (**10**); ▽ [(Me $_2$ SiCp) $_2$ Zr(Me)(THF)] $^+$ [B(C $_6$ F $_5$) $_4$] $^-$ (**9**); × [(Me $_5$ Cp) $_2$ ThMe] $^+$ [B(C $_6$ F $_5$) $_4$] $^-$ (**6**); ◆ [(Cp $_2$ ZrMe) $_2$ (μ -Me)] $^+$ [MePBB] $^-$ (**11**); ◇ [Me $_2$ C(Fluorenyl)(Cp)-ZrMe] $^+$ [FPBA] $^-$ (**4**); ▲ [*rac*-Et(Indenyl) $_2$ ZrMe] $^+$ [FPBA] $^-$ (**5**).

The low solubility of **9** in benzene- d_6 precludes investigation of the interionic structure, but taking advantage of the thermal stability, the 1D 1 H, 19 F HOESY spectrum was recorded in toluene- d_8 at 50 °C (concentration ca. 0.8 mM, *o*-F irradiation). The S/N ratio of this spectrum is not optimal, but as in complex **7**, interactions are detected between the *o*-F nuclei and the THF protons as well as with the H1 and H2 resonances. No interaction is observed between the *o*-F nuclei and the Zr-Me group.

Previous 1D 1 H NMR results²⁰ as well as our own HOESY data (vide infra) indicate that complex **10** must be formulated as a solvent adduct in solution. This compound is therefore considered to be an outer sphere ion-pair similar to **7** and **8** with the aromatic solvent acting as a weak ligand. Accordingly, its aggregation behavior is very similar to that of complexes **7**

and **8** (Figure 8b). In addition, the interionic structure of complex **10** was investigated in toluene- d_8 by irradiating the *o*-F resonance of the [B(C $_6$ F $_5$) $_4$] $^-$ counteranion. The corresponding 1D 1 H, 19 F HOESY spectrum is presented in Figure 9; the order of the interaction strength is Me(2) > Me(1) \gg Me(3) \approx *t*-Bu \gg Me(A), while no contact is observed for the Zr-Me group.

Complex **11**, in which the low coordinating ability of the [MePBB] $^-$ anion^{10c} ensures the formation of an outer sphere ion-pair, forms aggregates at increasing concentrations, albeit with a reduced tendency compared to **7**, **8**, and **10** (Figure 8c). Strong contacts are observed between the single Cp resonance of **11** and all the fluorine nuclei belonging to the disubstituted C $_6$ F $_4$ ring (in particular, the intensity of such interactions decreases in the order F6 \approx F5 > F4 > F3 \approx *o*-F). Complex **11** slowly decomposes in benzene- d_6 at room temperature, and

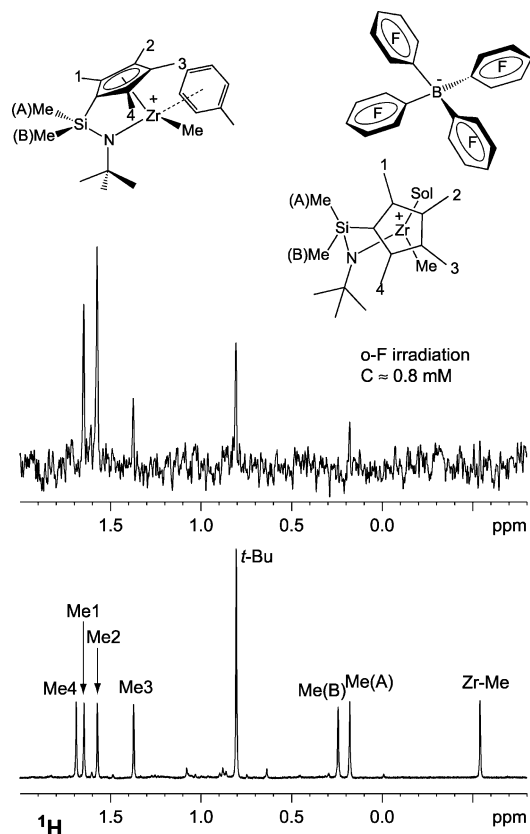
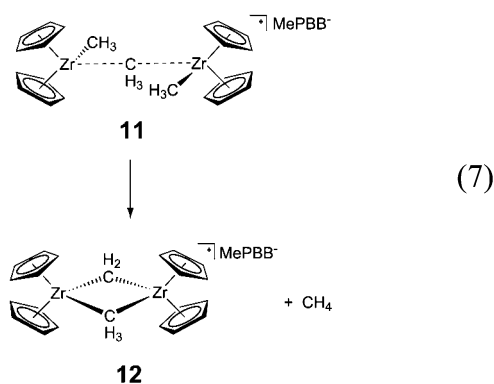


Figure 9. Proton (bottom) and 1D ^1H , ^{19}F HOESY spectra (*o*-F irradiation, top) of compound **10** (399.94 MHz, relaxation delay = 2 s, mixing time = 800 ms, 0.8 mM in toluene- d_6 , 298 K).

after several days a mixture of **11** and **12** is obtained, with concomitant methane formation (eq 7, see Supporting Information).⁴⁸



Even if it is slow, this elimination reaction is surprisingly clean at room temperature. In complex **12** the Cp protons (around 5.9 ppm) exhibit the same contacts as in **11**, but the inspection of the ^{19}F , ^1H HOESY spectrum reveals that the μ -methyl group now interacts with the fluorine nuclei in positions F6 and F5, while no interactions are detectable for the μ -CH₂ group (see Supporting Information).

Discussion

Inner Sphere Ion-Pairs. None of the ISIPs examined in this study exhibit detectable aggregation, irrespective of the cationic

or anionic moiety, suggesting that this is a general phenomenon for group 4 metallocenium inner sphere olefin polymerization catalyst ion-pairs. All the data (NOE, PGSE, and cryoscopy¹⁶) are consistent with a picture in which these systems exist in solution as 1:1 ion pairs. It is also evident that this behavior seems to be independent of concentration over the range 0.5–20 mM.¹⁶ In accordance with these observations, the ^1H , ^{19}F HOESY spectra of complexes **1**, **3**, and **5** indicate that a well-defined relative orientation predominates in solution consistent with the minimal tendency of ISIPs to aggregate.

In complexes **1** and **3**, the anion binds to the cation through a μ -Me group, and the phenyl rings are directed away from the cationic metal center. As expected, if for complex **1** the same relative cation–anion orientation is present in solution as found in the solid-state crystal structure,⁴⁹ only the B(C₆F₅)₃ fluorine nuclei at the *ortho* positions should be sufficiently proximate to the cation to undergo significant dipolar relaxation with the Cp protons, as is observed. Although a lack of NOE interaction does not always indicate a large internuclear distance,⁵⁰ two lines of reasoning lead us to suggest that the spectra shown in Figures 2 and 3 and in Supporting Information closely reflect the average structures in solution. First, changes in the cation–anion interionic orientation in other ion-pairs, also associated with aggregation, lead to the observation of interionic cross-peaks for the fluorine nuclei in the meta position (vide infra); second, the quantitative analysis (initial rate approximation³⁶) of the ^1H NOESY and ^1H , ^{19}F HOESY spectra in the case of complex **1** agree quite well with the reported crystal structure data (Table 2).

The approach used for interionic distance estimation here is based on the physically reasonable assumption that any internal motion is more rapid than the overall correlation time of the ion-pairs; in this case, the NOE-sensitive average internuclear distances can be estimated from the X-ray single crystal conformation in r^{-3} space.³⁶ As can be seen in Tables 2 and 3, in which the reported distances should be considered to have uncertainties of ca. 10%,⁵¹ this assumption appears to be valid when a terminal CH₃ group is considered. This is most likely due to the fact that rapid terminal CH₃ group internal rotation dominates the local value of the correlation time for any internuclear vector connecting this group with other groups. Using one of these average distances (e.g., the $\langle r \rangle_{\text{Zr-MeCp}}$ in the case of complex **1** and the $\langle r \rangle_{\text{Zr-MeH3}}$ in the case of complex **3**) all the other distances involving the terminal CH₃ groups are nicely reproduced. On the other hand, this simple assumption may be less valid when the average distance to be investigated does not involve freely rotating CH₃ groups. In the case of the *o*-F/Cp average distance in **1**, for example, neither the r^{-6} nor the r^{-3} average for the single X-ray conformer accurately reproduces the experimental data (Table 2).⁵²

The interionic structure of complex **5** is consistent, as expected, with the solid-state structure of the analogous compound [*rac*-Me₂Si(Indenyl)₂ZrMe]⁺[FPBA][−],^{10c} in that the FPBA[−] counteranion pairs with the cation via a strong Zr–F–

(49) Guzei, I. A.; Stockland, R. A.; Jordan, R. F. *Acta Crystallogr., Sect. C* **2000**, *56*, 635.

(50) In general the extent of NOE enhancement is not dependent on the internuclear distance alone. Factors such as the correlation time and the T_1 can prevent enhancement to an extent indistinguishable from background noise.

(51) For a discussion of the effects of internal motion on NOE-derived average distances, see ref 36, Chapter 5.

(48) For similar decomposition pathways see: (a) Brownie, J. H.; Baird, M. C.; Zakharov, L. N.; Rheingold, A. L. *Organometallics* **2003**, *22*, 33. (b) Zhang, S.; Piers, W. E. *Organometallics* **2001**, *20*, 2088. (c) Bochmann, M.; Cuenca, T.; Hardy, D. T. *J. Organomet. Chem.* **1994**, *484*, C10.

Al interaction as indicated by a strong cross-peak with the adjacent Zr-Me group (Figure 4; see Supporting Information for additional details). However, the presence of two diastereomers with some overlapping signals in the ^1H spectrum makes it difficult to describe in detail the network of the interionic dipolar interactions. In addition to the Al-F group, the F6, F5, and *o*-F* nuclei can interact with different protons on the metal cation (the ^{19}F resonances are assigned by means of standard ^{19}F COSY and ^{19}F NOESY experiments), and the general trend indicates that the F6 interaction is, not surprisingly, the strongest (Figure 4). Interestingly, there is a strong homonuclear NOE interaction between the F6 and the *o*-F* atoms on the counteranion. This contact is not expected to come from within the same biphenyl moiety as confirmed by a similar ^{19}F NOESY experiment on the simple $[\text{Ph}_3\text{C}]^+[\text{FPBA}]^-$ salt. Rather, this interaction is likely indicative of π -stacking between one C_6F_4 ring and a C_6F_5 ring of an adjacent biphenyl similar to that observed in the solid state.^{3c}

The results of these homo- and heteronuclear NOE investigations on inner sphere intimate ion-pairs such as complexes **1–5** are in agreement with previous investigations using simple ^1H and/or ^{19}F NMR spectroscopy and arguing from chemical shift displacement accompanying coordination. For example, the chemical shift of the bridging fluorine is an excellent indicator of $\text{M}\cdots\text{F}-\text{Al}$ coordination,^{10c} while changes in the *m*-F vs *p*-F chemical shift difference reflect coordination of the $[\text{RB}(\text{C}_6\text{F}_5)_3]^-$ anions.^{18,29,53} These data can be interpreted in a straightforward way: the changes in chemical shifts reflect the strength of the anion-cation coordinative interaction and are in general related to an interplay of steric and electronic constraints at both cation and anion.^{2e,10c,12b} In addition, there are now a number of X-ray diffraction studies for this class of compounds from which detailed metrical parameters can be analyzed and compared.⁹ Theoretical calculations at the ab initio level indicate that the cation-anion interaction in these systems is primarily electrostatic in nature,^{11a,c} but the residual coordinative ability of the anion is sufficient to enforce a localized anion/cation geometry. It is therefore likely that the X-ray-derived solid-state structures of ISIPs are a reasonable approximation of the solution-state structures in low-polarity solvents. This conclusion is also in good agreement with the “gas-phase” and solvated ground-state geometries computed in theoretical studies.¹¹

Outer Sphere Ion-Pairs. Far more difficult is the solution structural characterization of species in which the anions are not coordinated to/strongly interacting with, the formally

unsaturated cations. These species, containing very weakly coordinating counteranions, are likely to exist as solvent-separated ion-pairs in solvents with relatively high permittivities such as bromobenzene ($\epsilon_r^{293} = 5.45$), chlorobenzene ($\epsilon_r^{293} = 5.69$), and methylene chloride ($\epsilon_r^{298} = 8.93$). However, indirect evidence and classical calculations based on the theory of Fuoss⁵⁴ indicate that these complexes should behave as intimate ion-pairs in the relatively low-permittivity solvents typically used in single-site polymerization reactions (i.e., benzene, toluene, and saturated hydrocarbon solvents).⁵⁵ Accordingly, recent work by Landis,^{12b} Bochmann,⁸ Waymouth,⁵⁶ and Busico,⁵ as well as recent results from our laboratory,^{2e,3b-d,10,19} conclusively demonstrates that the ion-pairs are the effective propagation species and that the anion cannot be considered as a mere spectator during the enchainment process. In fact, in the classical scenario of a two-step Cossee-type mechanism,¹⁵ consisting of a series of equilibria in which reversible alkene association is followed by alkene insertion into the polymeryl σ -bond, the present OSIPs plausibly model one component of this equilibrium and consequently, together with the zirconocenium-polymeryl anion ISIP, the resting state of the catalyst. It has already been shown that the first step in the formation of catalytically active species in metallocene-mediated polymerization of simple olefins is likely to be a monomer association/dissociation preequilibrium involving the electron-deficient metallocenium center.⁵⁷ On the other hand, nonchelated alkyl-alkene cationic group 4 d^0 complexes have not been directly observed so far. In addition, as asserted by Busico, “for a monomer molecule to insert, it is assumed that the anion must be partly displaced, but to where exactly is hard to say.”^{5a} With the aim of better understanding the cation-anion interplay after generation of the putative catalytically active species, we applied the combined NOE and PGSE techniques to the ion-pairs formed via anion displacement by a Lewis base. Relatively strong Lewis bases have been used in several instances to stabilize cationic zirconocene complexes,^{29,58} while weaker Lewis bases have been employed to study the equilibria and kinetics of anion displacement reactions.²⁸ The use of moderately strong Lewis bases (i.e.,

- (52) Experimental methods to estimate the actual value of the local correlation time rely on measurement of the dipolar contribution to the ^{13}C relaxation time (see, for example: (a) Gaemers, S.; van Slageren, J.; O'Connor, C. M.; Vos, J. G.; Hage, R.; Elsevier, C. J. *Organometallics* **1999**, *18*, 5238. (b) Bühl, M.; Hopp, J.; von Philipsborn, W.; Beck, S.; Proscen, M. H.; Rief, U.; Brintzinger, H.-H. *Organometallics* **1996**, *15*, 778. (c) Abragam, A. *The Principles of Nuclear Magnetism*; Clarendon Press: Oxford, 1961) or on estimation of the homo- or heteronuclear NOE response at different temperatures (see, for example: (d) Macchioni, A.; Magistrato, A.; Orabona, I.; Ruffo, F.; Röthlisberger, U.; Zuccaccia C. *New J. Chem.* **2003**, *27*, 455. (e) Zuccaccia, C.; Bellachioma, G.; Cardaci, G.; Macchioni, A. *J. Am. Chem. Soc.* **2001**, *123*, 11020). A more in-depth analysis could, in principle, be achieved using the two-dimensional conformer population analysis algorithm proposed by Landis and co-workers (see, for example: (f) Casey, C. P.; Hallenbeck, S. L.; Wright, J. M.; Landis, C. R. *J. Am. Chem. Soc.* **1997**, *119*, 9680. (g) Landis, C. R.; Luck, L.; Wright, J. M. *J. Magn. Reson., Ser. B* **1995**, *109*, 44. (h) Landis, C.; Allured, V. S. *J. Am. Chem. Soc.* **1991**, *113*, 9493), but this is beyond the scope of the present work.
- (53) (a) Hayes, P. G.; Welch, G. C.; Emslie, D. J. H.; Noack, C. L.; Piers, W. E.; Parvez, M. *Organometallics* **2003**, *22*, 1577. (b) Horton, A. D.; de With, J. *Organometallics* **1997**, *16*, 5424.

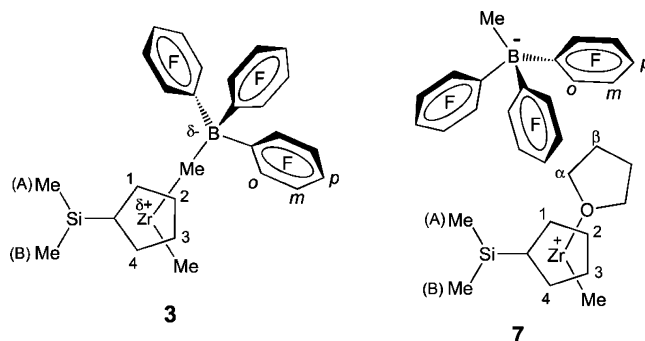
- (54) Fuoss, R. M. *J. Am. Chem. Soc.* **1958**, *80*, 5059.
- (55) Computational studies (see refs 11a and 30) show that multiple geometries are energetically accessible, and the cation-anion interactions in these kinds of ion-pairs are poorly localized. On the other hand, it has been proposed that NOE is sensitive in distinguishing between conformations differing by only a few kJ/mol (see ref 52d).
- (56) Wilmes, G. M.; Polse, J. L.; Waymouth, R. M. *Macromolecules* **2002**, *35*, 6766.
- (57) (a) Dalmann, M.; Erker, G.; Bergander, K. *J. Am. Chem. Soc.* **2000**, *122*, 7986. (b) Karl, J.; Dalmann, M.; Erker, G.; Bergander, K. *J. Am. Chem. Soc.* **1998**, *120*, 5643. (c) Galakhov, M. V.; Heinz, G.; Royo, P. *Chem. Commun.* **1998**, *1*, 17. (d) Wu, Z.; Jordan, R. F.; Petersen, J. L. *J. Am. Chem. Soc.* **1995**, *117*, 5867. (e) Casey, C. P.; Hallenbeck, S. L.; Pollok, D. W.; Landis, C. R. *J. Am. Chem. Soc.* **1995**, *117*, 9770.
- (58) (a) Carpentier, J.-F.; Maryin, V. P.; Lucy, J.; Jordan, R. F. *J. Am. Chem. Soc.* **2001**, *123*, 898. (b) Ringelberg, S. N.; Meetsma, A.; Hessen, B.; Teuben, J. H. *J. Am. Chem. Soc.* **1999**, *121*, 6082. (c) Witte, P. T.; Meetsma, A.; Hessen, B.; Budzeelar, P. H. M. *J. Am. Chem. Soc.* **1997**, *119*, 10561. (d) Alelyunas, Y. W.; Baenziger, N. C.; Bradley, P. K.; Jordan, R. F. *Organometallics* **1994**, *13*, 148. (e) Alelyunas, Y. W.; Guo, Z.; LaPointe, R. E.; Jordan, R. F. *Organometallics* **1993**, *12*, 544. (f) Eshuis, J. J. W.; Tan, Y. Y.; Meetsma, A.; Teuben, J. H. *Organometallics* **1992**, *11*, 362. (g) Burrowsky, S. L.; Jordan, R. F.; Hinch, G. D. *Organometallics* **1991**, *10*, 1268. (h) Alelyunas, Y. W.; Jordan, R. F.; Echols, S. F.; Borkowsky, S. L.; Bradley, P. K. *Organometallics* **1991**, *10*, 1406. (i) Jordan, R. F.; Bradley, P. K.; Baenziger, N. C.; LaPointe, R. E. *J. Am. Chem. Soc.* **1990**, *112*, 1289. (j) Eshuis, J. J. W.; Tan, Y. Y.; Teuben, J. H. *J. Mol. Catal.* **1990**, *62*, 277. (k) Jordan, R. F.; Guram, A. S. *Organometallics* **1990**, *9*, 2116. (l) Jordan, R. F.; LaPointe, R. E.; Bradley, P. K.; Baenziger, N. *Organometallics* **1989**, *8*, 2892. (m) Taube, R.; Krukowa, L. *J. Organomet. Chem.* **1988**, *347*, C9. (n) Jordan, R. F.; Bajgur, C. S.; Dasher, W. E. *Organometallics* **1987**, *6*, 1041. (o) Jordan, R. F.; Bajgur, C. S.; Willett, R.; Scott, B. *J. Am. Chem. Soc.* **1986**, *108*, 7410.

THF, PPh₃) is preferred for the present model complex investigation, in that the anion displacement equilibrium lies far to the right (toward the Lewis base adduct) and affords stable compounds suitable for long-duration NMR experiments such as ¹⁹F, ¹H HOESY. In fact, formation of ion-pairs **7** and **8** proceeds quickly and cleanly after addition of one equivalent of THF or PPh₃, respectively, to complex **3** to afford new ion-pairs in which the anion is relegated to the second coordination sphere. Brintzinger and co-workers have shown that reaction of some ion-pairs with various Lewis bases proceeds with large negative values of ΔS° , providing convincing indirect evidence that the anion remains associated with the cation in benzene solution.²⁸ The present observation of interionic dipolar interactions in the ¹H NOESY and ¹⁹F, ¹H HOESY spectra of **7** and **8** directly indicate that intimate ion-pairs are formed, the solution interionic structures of which are investigated here for the first time.

In the case of complex **7** (1.7 mM), the dipolar interionic contact between the B-Me group and cation H1 protons is detectable in the ¹H NOESY spectrum (Figure 5).⁵⁹ In addition, specific cation–anion interactions were also observed in the corresponding ¹⁹F, ¹H HOESY spectrum (Figure 6). Taken together, these data prove directly that the displacement of the anion by the THF generates an intimate OSIP in which the anion is preferentially localized on the THF side of the cation, shifted slightly toward the Me(A) group and further away from the Zr-Me group as indicated by the increased interaction with H1. The absence of interactions between the B-Me group and α^60 and β THF and Me(A) protons seems to indicate a favored anion orientation in which the B-Me moiety points away from the metal center. In contrast to precursor complex **3**, interionic contacts in complex **7** are detected not only for the *o*-F, but also for the *m*-F fluorine nuclei (Figure 6). Interestingly, the specificity in the interionic interactions is not affected by an increase in concentration (from 1.0 to 1.7 mM) even though PGSE data indicate formation of aggregates (vide infra). In an effort to determine if the B-Me/H1 contact could be due to aggregation phenomena, ¹H NOESY and a 1D GOESY³² (H1 irradiation, Figure 5c) experiments were attempted at ca. 0.6 mM, where PGSE measurements indicate the presence of mainly 1:1 ion-pairs (*N* ≈ 1). Unfortunately, the S/N ratio is insufficient to conclude unambiguously that the observed B-Me/H1 cross-peak arises from aggregation.⁶¹ In light of the parallel PGSE results it was decided to limit the quantitative analysis to compound **7** and to continue to investigate all the other systems from a semiquantitative point of view (i.e., the spectra were not rigorously recorded in the initial rate approximation regime).

Quantitative ¹H–¹H (Figure 5) and ¹H, ¹⁹F (see Supporting Information) analyses for a 1.7 mM solution of **7**, using an approach similar to that discussed above, afford the data reported

in Table 4. The average distance between the B-Me group on the anion and the H1 protons on the cation is estimated to be 4.1 Å, while the average distance between the same cation nuclei and the *o*-F fluorine on the anion is estimated to be 4.5 Å. Thus, in contrast to parent compound **3** (Table 3), the anion B-Me and the *o*-F groups in the Lewis base complexes are ca. 1.1 and ca. 0.4 Å more distant, respectively, from the closest cation proton (H1 in **7** and H2 in **3**).



These data strongly suggest that in complex **7** the anion is energetically freer to assume various orientations with respect to the cation, as expected in the absence of localized coordinative interactions. On the other hand, the relative anion–cation position is well defined, with the anion localized primarily on the side of the cation to which THF is coordinated and shifted toward the backside of the metallocenium cation. Computationally optimized interionic structures for analogous metallocenium–olefin adducts (namely, [Cp₂ZrMe(C₂H₄)]⁺[MeB(C₆F₅)₃][−]) are in excellent qualitative agreement with the experimental data reported here.⁶² In addition, using the data reported in Table 4 and the Zr–H1 distance (3 Å) from the X-ray structure of complex **9** (see below), we can roughly estimate, in the most extreme situation of a linear B–H1–Zr alignment, that the Zr–B distance is ca. 7.2–7.3 Å. The corresponding DFT-derived Zr–B distance calculated for the compound [Cp₂ZrMe(C₂H₄)]⁺[MeB(C₆F₅)₃][−] is 6.7 Å,⁶² while the corresponding ab initio-derived distance is 7.4 Å in the related complex [H₂Si(C₅H₄)(*t*-BuN)Ti(Me)(C₂H₄)]⁺[MeB(C₆F₅)₃][−].^{11a}

In contrast to complex **7**, the interionic structure of complex **8** at 2.4 mM is substantially less localized than that at 1.1 mM (Figure 7). This behavior can be understood by the results of detailed concentration-dependent PGSE NMR investigations for both ion-pairs **8** (0.1–3.1 mM) and **7** (0.1–2.2 mM) in that a concentration dependence of the observed interionic interactions might be a consequence of aggregation. As noted previously in the literature for similar compounds (and in the present Experimental Section),^{18,20,29} OSIPs **7** and **8**, synthesized in situ, begin to separate as finely dispersed oily phases at higher concentrations, generating new sets of resonances with different chemical shifts (probably due to the changes in the local diamagnetic susceptibility in the new nonmonodisperse phase⁶³). The highest concentrations used in this work, determined by integration with respect to an internal standard, refer to the

(59) Note that these NOESY spectra were recorded with a 6 s relaxation delay, 150 ms mixing time, and 32 scans per increment. If the parameters routinely used for small molecule NOESY experiments (namely 1 s relaxation delay, 800 ms mixing time, and 16 scans per increment) are employed, the B-Me/H1 cross-peak is hardly visible. This is likely a consequence of the rapid B-Me relaxation time in combination with the expectation of very little NOE enhancement.

(60) The cross-peak corresponding to the F2 α resonance and to the F1 B-Me resonance visible in Figure 5 is most probably an artifact in that the corresponding mirror image peak across the diagonal is not observed.

(61) The 2D-NOESY experiment (Figure 5, a and b) and the 1D-GOESY experiment (Figure 5c) were acquired in the initial rate approximation.

(62) Nifant'ev, I. E.; Ustynuk, L. Y.; Laikov, D. N. *Organometallics* **2001**, *20*, 5375.

(63) Preliminary NMR results obtained for [(1,2-Me₂Cp)₂ZrMe(PPh₃)]⁺[MeB(C₆F₅)₃][−] indicate a benzene:metallocenium ion-pair mole ratio of ca. 20:1 within the oily phase that separates completely from benzene solution.

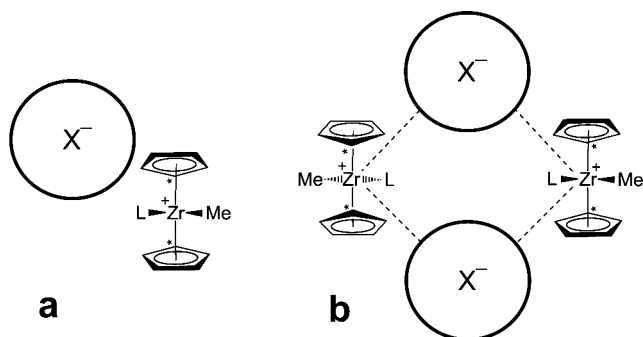


Figure 10. Proposed average solution structures of ion-pair (a) and ion-quadruple (b) for the outer sphere ion-pairs **7** and **8**. These structures are consistent with both the NOE and PGSE data. The asterisks indicate the carbon atoms to which the silicon bridge is connected.

portion of the ion-pairs still homogeneously dissolved in the benzene- d_6 solution and must be considered to be the concentration of a saturated solution.

As can be seen from Figure 8a, complexes **7** and **8** exhibit a markedly higher tendency to aggregate than parent complex **3**. It is quite surprising that the interionic structure of complex **7** retains a high degree of localization while the corresponding aggregation number indicates a substantial presence of ion-quadruples at 1.7 mM concentration ($N = 1.56$, Table 5). A possible explanation for this behavior is that the average solution structure of the ion-quadruple formed by **7** at higher concentrations is the one depicted in Figure 10.⁶⁴ By reasonably assuming that the ion-quadruple structures of **7** and **8** are the same, we suggest that the observed lower level of specificity in the anion–cation interaction for a 2.4 mM solution of **8** ($N = 1.95$, Table 5) must be attributed to the partial formation of ion-hextuples that cannot form, starting from ion-quadruples, without leading to a loss of structural localization.⁶⁵ The fact that complexes **7** and **8** exhibit a completely different solution-structural behavior than previously investigated ion-pairs **1–6** does suggest that there is a pervasive modification of properties on transition from inner- to outer sphere metalocenium ion pairs. To further test this hypothesis, concentration-dependent PGSE measurements were extended to compounds **2**, **3**, **4**, and **5** (ISIPs) and to complexes **9**, **10**, and **11** (OSIPs).

Beck et al. initially communicated evidence that aggregation may be an important consideration in group 4 metalocenium ion-pairs.⁶⁶ We have recently shown that aggregation is not

important for ISIPs,¹⁶ and we now extend this work to OSIPs. The results reported here for a wide-spectrum ion-pairs support the following general conclusion: ISIPs do not aggregate to a detectable extent in low-polarity hydrocarbon solvents, whereas OSIPs can aggregate significantly at concentrations above approximately 5×10^{-4} M. Furthermore, the extent to which OSIPs aggregate is a function of the cation ligand framework as well as the structure of the counteranion.

The behavior of complex **9** deserves additional comments. The X-ray analysis in the solid-state (see below) and the solution-phase NMR data are consistent with a formulation of compound **9** as discrete cationic and anionic fragments (an outer sphere ion-pair). Unfortunately, **9** is sparingly soluble (saturated solution ca. 0.4 mM), and consequently, its aggregation tendency cannot be fully explored. Some indication of aggregation can be observed when an excess of **9** is heated in refluxing benzene- d_6 for about 1.0 min (Figure 8c). In this case, a metastable supersaturated solution can be prepared, but as expected, crystals form over a period of a few hours, rendering the measurement of the diffusion coefficient necessarily imprecise (i.e., the actual concentration cannot be defined, and signal intensities decrease because of the concomitant precipitation). As for the interionic structure, the results obtained for complex **9** are very similar to those for complex **7**: the anion is localized on the side of the cation closer to the H1 protons. The low intensity of the signals in the 1D ^1H , ^{19}F HOESY spectrum recorded at 50 °C (*o*-F irradiation, see Supporting Information) suggests weaker ion-pairing in **9** vs that in parent compound **7**, but this could also be due to reduced cross-relaxation efficiency due to a decrease in the correlation time.

Complex **10** exhibits a behavior very similar to that of complexes **7** and **8** although with somewhat greater tendency for aggregation. Interestingly, **10** is reasonably stable in toluene- d_8 but appears to decompose more rapidly in benzene- d_6 at concentrations greater than ca. 0.6 mM. The 1D ^1H , ^{19}F HOESY spectrum (*o*-F irradiation, Figure 9) was recorded at 0.8 mM in toluene- d_8 to take advantage of the higher sample stability.⁶⁷ In accordance with the formulation of this compound and in accordance with the aforementioned results on complexes **7** and **8**, the interionic structure of **10** exhibits pronounced localization, with the anion predominantly residing on the side of the cation opposite to the Zr-Me, as confirmed by observation of a small interaction with the Me(A) group and the absence of any interaction with the Zr-Me moiety. The observation that Me(2) interacts with the anion more strongly than the *t*-Bu group, and the lack of the Zr-Me interaction, are also in agreement with the presence of a solvent molecule in the formally vacant coordination site. A structure in which the $[\text{B}(\text{C}_6\text{F}_5)_4]^-$ anion is in the second coordination sphere of the Zr center is also consistent when these data are compared with the ^{19}F , ^1H HOESY data for the Th-containing ion-pair **6**. For the latter, the ^{19}F , ^1H HOESY results confirm the interaction between the anion and the Th-Me group, as expected

(64) That structures similar to that sketched in Figure 10 for ion-quadruples are in fact accessible is supported by the crystal-structure packing in similar compounds: (a) Gibson, V. C.; Humphries, M. J.; Tellmann, K. P.; Wass, D. F.; White, A. J. P.; Williams, D. J. *Chem. Commun.* **2001**, 2252. (b) Chernega, A.; Cook, J.; Green, M. L.; Labella, L.; Simpson, S. J.; Souter, J.; Stephens, A. H. *J. Chem. Soc., Dalton Trans.* **1997**, 3225. (c) Amorose, D. M.; Lee, R. A.; Petersen, J. L. *Organometallics* **1991**, *10*, 2191.

(65) Another interpretation that cannot be ruled out is that the average solution interionic structures in ion-quadruples formed by complexes **7** and **8** are substantially different. In addition, it could be argued that the observed lower level of localization arises from an increased rate of site epimerization that exchanges the magnetically nonequivalent protons (H1/H4, H2/H3, Me(A)/Me(B)). We are confident that the observed nonspecific interactions reflect the actual quasi-static structure in solution for two principal reasons: (1) Reported rates for site epimerization in complexes similar to complex **8** are on the order of 0.1 s^{-1} , (i.e., too slow to satisfy the condition of fast exchange on the relaxation time scale (see ref 36) necessary to produce the spectrum reported in Figure 7). (2) In accordance with point 1, ^1H NOESY spectra of complex **8** recorded with the same mixing time do not exhibit evidence for additional NOE enhancement (H1 with H3 and H2 with H4) due to H1/H4 and H2/H3 exchanges.

(66) Beck, S.; Geyer, A.; Brintzinger, H.-H. *Chem. Commun.* **1999**, 24, 2477.

(67) The higher stability of compound **10** in toluene could be due in principle to either (1) a higher intrinsic stability due to coordination of toluene instead of benzene (see, for example: Hayes, P. G.; Piers, W. E.; Paervez, M. J. *Am. Chem. Soc.* **2003**, *125*, 5622) or (2) a lower level of aggregation that impedes possible bimolecular decomposition pathways (see, for example: Li, L.; Hung, M.; Xue, Z. *J. Am. Chem. Soc.* **1995**, *117*, 12746) or, more likely, (3) a combination of 1 and 2.

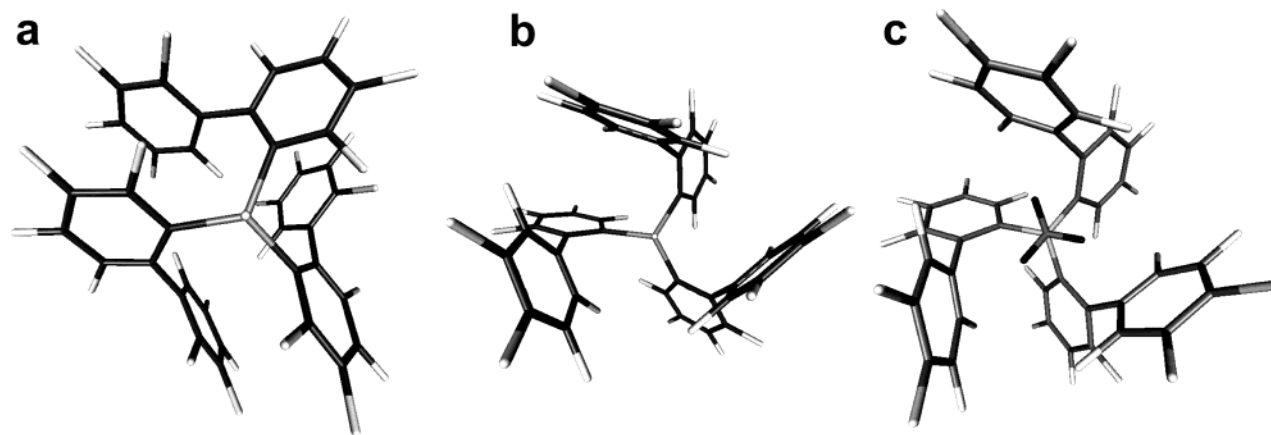
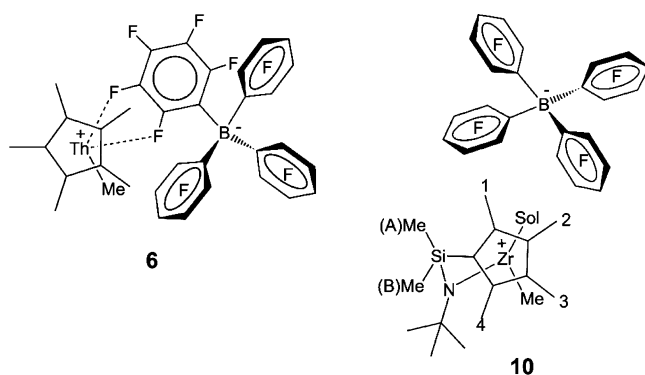


Figure 11. X-ray-derived stick representations of the [FPBA][−] and [MePBB][−] anions, taken from refs 10c and 10d. (a) “Coordinated” [FPBA][−] viewed along the F–Al bond in complex [(Me₂Si(Me₄Cp)(*t*-BuN)Zr(Me))⁺][FPBA][−], (b) “Free” [FPBA][−] viewed along the F–Al bond in compound [Ph₃C]⁺[FPBA][−]. (c) [MePBB][−] viewed along the CH₃–B bond in compound [((1,2-Me₂Cp)₂ZrMe)₂(μ-Me)]⁺[MePBB][−]. The cationic moieties have been omitted for the purpose of clarity.

if the solid-state structure is primarily retained in solution, adding evidence for the formulation of **6** as an inner sphere ion-pair.⁶⁸



The interionic structure of binuclear complex **11**, due to the simplicity of the metal cation, allows us to focus on the weak coordinative properties of the [MePBB][−] anion.^{2e,10c} The anion is localized on the side of the cation proximate to the Cp ligands as demonstrated by the absence of any hydrogen–fluorine interaction with either the μ-methyl or the terminal methyl groups. In addition, proton–proton interactions are not observed in the ¹H NOESY spectrum. To elucidate the relative anion orientation with respect to the cation, the structure of the [MePBB][−] anion must be taken into account. Unlike [FPBA][−], [MePBB][−] does not coordinate to the Zr center,⁶⁹ and after methide abstraction by the PBB Lewis acid cocatalyst from the Zr dimethyl precursor, the geometry of the anion is similar to that of the “free” [FPBA][−] anion with the C₆F₅ rings of the biphenyl groups shielding the B–Me group (Figure 11). Consequently, the B–Me group cannot interact with the cationic protons, even if directed toward them. However, the relative cation–anion orientations can be probed in solution by means of ¹⁹F,¹H HOESY spectroscopy.⁷⁰ In fact, one of the two

nonequivalent *o*-F atoms interacts strongly with the B–Me group but not with the cation ligand protons, while the other *o*-F atom is the only one on the C₆F₅ fragment that exhibits interionic interaction with the cation. The additional observation that the relative strength of interionic interactions between Cp protons and the anion C₆F₄ fluorine nuclei follows the order F₆ ≈ F₅ > F₄ > F₃ conclusively demonstrates that in complex **11** the B–Me vector of the [MePBB][−] anion is directed away from the metal center in a manner similar to that found in the solid state for the analogous [((1,2-Me₂Cp)₂ZrMe)₂(μ-Me)]⁺[MePBB][−] complex.^{10c}

The observation of a different interionic structure on passing from **11** to **12** reflects the large changes in the electronic charge distribution on the cationic moiety and simultaneously illustrates that the HOESY experiment is very sensitive to detecting these changes. In fact, the anion is localized on the μ-CH₃ side of the metallocene distal to the μ-CH₂ group, and as in the case of **11**, the B–Me vector of the [MePBB][−] anion is directed away from the metal center. Note that in the case of **12** or related complexes, even with X-ray structural data in hand, it might be difficult to determine the exact location of the anion with respect to the cation due to the known difficulties in resolving disorders frequently associated with similar bridging ligands.^{48a,b}

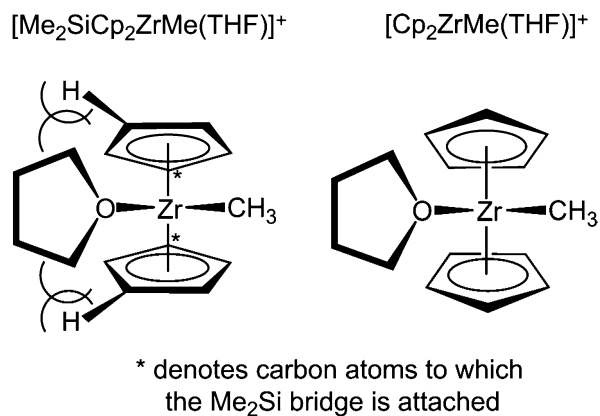
Crystal Structure of [(Me₂SiCp₂)Zr(Me)(THF)]⁺[B(C₆F₅)₄][−] (9**).** In complex **9**, the coordination environment around the Zr atom consists of the silicon-bridged bis-η⁵-cyclopentadienyl ligand, a methyl ligand, and an η¹-oxygen-bound THF ligand, affording the expected pseudotetrahedral metallocenium geometry at Zr (Figure 12). The Zr–CH₃ distance is 2.259(5) Å, the Zr–O distance is 2.210(3) Å, and the CH₃–Zr–O angle is 96.8°. While the Zr–CH₃ distance and the CH₃–Zr–O angle are very similar to the corresponding values observed for [Cp₂ZrMe-(THF)]⁺[BPh₄][−] by Jordan and co-workers (2.256(10) Å and 97.4°),^{58o} the Zr–O bond distance and the THF arrangement are distinctly different. That is, the Zr–O bond distance is ca. 0.1 Å longer (2.210(3) Å vs (2.122(14) Å), and the torsion angles for the two C_{methyl}–Zr–O_{THF}–C_{α,THF} linkages are 36.3° and −153.7°, which places the THF molecule roughly 31.3°

(68) Another possibility for **6** is to assume it forms an OSIP in which there is a lower degree of specificity in the anion–cation interaction. While this hypothesis is difficult to substantiate due to the NMR equivalence of the Cp-methyl resonances, it seems very unlikely in the context of the behavior of all the other ion-pairs investigated in this work.

(69) The same non-coordinative characteristics are observed in the case of [FPBB][−] (FPBB = tris(2,2',2''-nonafluorobiphenyl)fluoroborate, unpublished results from this laboratory), suggesting that the central atom (B versus Al) plays a fundamental role.

(70) This should be true also in the case of “free” [FPBA][−], but the rapid relaxation of the Al-F resonance precludes further investigations by ¹⁹F NOESY experiments.

out of the plane described by atoms C_{methyl} , Zr, and O_{THF} . This result is in contrast to the nearly perpendicular arrangement (77.7°) reported for $[\text{Cp}_2\text{ZrMe}(\text{THF})]^+[\text{BPh}_4]^-$.^{58o} However, THF orientations similar to those in **9** are observed in $[(\text{Me}_5\text{Cp})_2\text{Zr}(\text{CH}_2\text{SiMe}_3)(\text{THF})]^+[\text{BPh}_4]^-$ by Petersen and co-workers^{64c} and for $[(\text{Me}_5\text{Cp})_2\text{TiMe}(\text{THF})]^+[\text{BPh}_4]^-$ by Bochmann and co-workers.⁷¹ A rationale for the different THF orientations in these compounds vs that in $[\text{Cp}_2\text{ZrMe}(\text{THF})]^+[\text{BPh}_4]^-$ has been presented.^{64c} The steric hindrance exerted by the pentamethyl-substituted cyclopentadienyl rings prevents the THF from achieving the perpendicular orientation necessary for good overlap between the O π -donor orbital primarily of p character and the vacant Cp_2Zr hybridized d orbital of a_1 symmetry,⁷² resulting in a weaker interaction and longer Zr–O distance. In the present case, the Zr–O distance of 2.210(3) Å is closer to that of $[(\text{Me}_5\text{Cp})_2\text{Zr}(\text{CH}_2\text{SiMe}_3)(\text{THF})]^+[\text{BPh}_4]^-$ (2.243(3) Å).^{64c} The same steric argument appears sufficient to explain the THF orientation/bonding found in **9**. On one hand, complex **9** presents an even more open coordination sphere ($\text{Cp}_{\text{centroid}}\text{--Zr--Cp}_{\text{centroid}}$ angle = 126.54°) at the Zr vs $[\text{Cp}_2\text{ZrMe}(\text{THF})]^+[\text{BPh}_4]^-$ ($\text{Cp}_{\text{centroid}}\text{--Zr--Cp}_{\text{centroid}}$ angle = 129.59°), suggesting there is more space to accommodate the THF ligand in the perpendicular orientation. On the other hand, the bridging Me_2Si group prevents free Cp ring rotation, and the minimal steric hindrance provided by the hydrogens on the Cp ring β position (H2 and H10) cannot be released until the THF is rotated at least partially toward the electronically less favorable “parallel” orientation.



Regarding preferential ion-pairing in the solid state, of the three nearest-neighbor anions of a given cation in the crystal of **9**, none are positioned such that they would produce the observed NOE interactions in solution, where the preferred anion position is proximate (*syn*) to the THF ligand (see above). In particular, the B atom of the nearest anion ($\text{Zr--B} = 7.021 \text{ \AA}$) is located midway between the CH_3 and the THF ligands, displaced ca. 26° from the plane described by C_{methyl} , Zr, O_{THF} (Figure 12). The B atom of the second-nearest anion ($\text{Zr--B} = 7.254 \text{ \AA}$) is positioned approximately *anti* to the THF ligand and lies ca. 35.7° out of the same plane but in the opposite direction. In addition, solvent molecules (benzene) closest to a given Zr atom are positioned approximately *anti* to the CH_3 ligand. While it will require further investigations, the presence

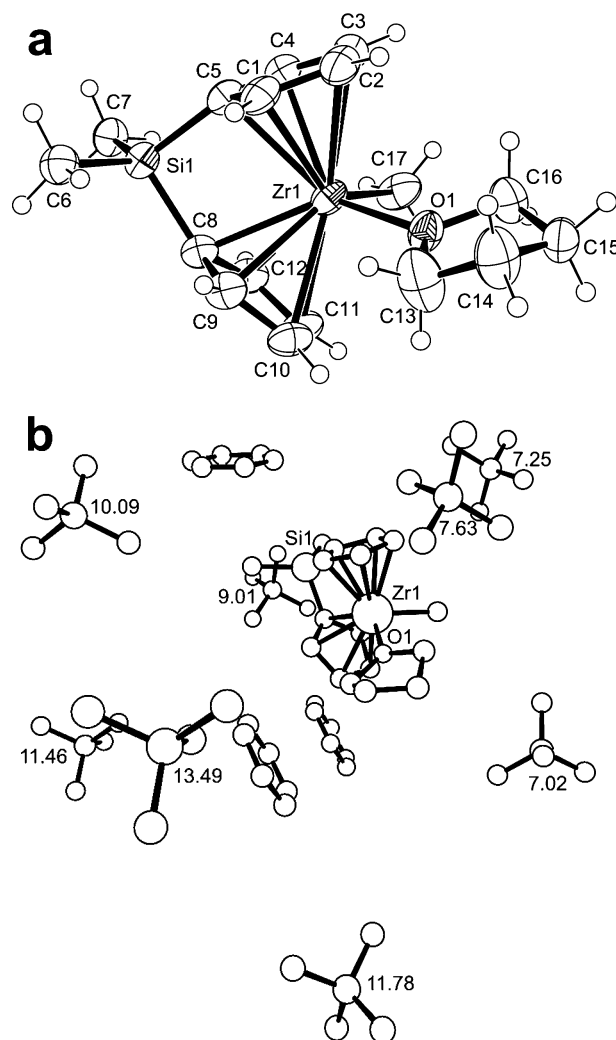


Figure 12. (a) ORTEP drawing of the cationic part of complex $[(\text{Me}_2\text{SiCp}_2)\text{Zr}(\text{Me})(\text{THF})]^+[\text{B}(\text{C}_6\text{F}_5)_4]^- \cdot \text{C}_6\text{H}_6$ (**9**) with thermal ellipsoids plot (50% probability for all non-hydrogen atoms). (b) PLUTO drawing showing the position of the nearest-neighbor anions and solvent molecules to a given cation in the crystal of **9**. The number reported next to each anion, represented here by the $\text{B}(\text{C}_{\text{ipso}})_4$ unit, is the Zr–B distance in Å. Hydrogen atoms are omitted for clarity. Both drawings were created using the ORTEP-3 for Windows; Farrugia, L. J. *J. Appl. Crystallogr.* **1997**, *30*, 565.

in the solid state of solvent molecules occupying the solution anion-preferred face of the cation suggests another possible, intriguing explanation for the observed weak NOE intensity arising from cation–anion interactions in solution: it is possible that the solvent preference for this face of the cation persists in solution, i.e., the solution ion-pair is solvent-separated. Correlation between the average interionic solution structure and the most stable ion-pairing found in the solid state is non-trivial, requiring daunting calculations of electrostatic and the “steric” contributions to the total energy for each ionic pair found in the solid state.⁷³

Conclusions

The results reported here show, for the first time, that application of complementary NOE and PGSE methodologies

(71) Bochmann, M.; Jagger, A. J.; Wilson, L. M.; Hursthouse, M. B.; Motevalli, M. *Polyhedron* **1989**, *8*, 1838.

(72) Lauher, J. W.; Hoffmann, R. *J. Am. Chem. Soc.* **1976**, *98*, 1729.

(73) (a) Gruet, K.; Clot, E.; Eisenstein, O.; Lee, D. H.; Patel, B.; Macchioni, A.; Crabtree, R. H. *New J. Chem.* **2003**, *27*, 80. (b) Macchioni, A.; Zuccaccia, C.; Clot, E.; Gruet, K.; Crabtree, R. H. *Organometallics* **2001**, *20*, 2367. (c) Macchioni, A.; Bellachioma, G.; Cardaci, G.; Cruciani, G.; Foresti, E.; Sabatino, P.; Zuccaccia, C. *Organometallics* **1998**, *17*, 5549.

to group 4 metallocenium polymerization catalyst ion-pairs affords unambiguous information concerning solution-phase interionic structure and aggregation. Both features are found to be dependent on whether the counteranion is in the inner or outer coordination sphere. In the case of ISIPs, the derived interionic solution structures are in excellent agreement with those in the solid state, and there is no detectable ion-pair aggregation. In other words, the residual coordinative character of the cation–anion interaction is sufficiently strong to enforce a relatively low degree of ion-pair mobility, and thus the solid-state, structurally frozen regime represents a good approximation of the relative anion–cation orientation in solution. The same residual coordinative interaction also tends to reduce the separated ion character of these systems, which accounts for the minimal aggregation observed in benzene solution, even at fairly high concentrations (10–20 mM).

In the case of outer sphere ion-pairs, the anion is localized proximate to the cation in a position different from that in the ISIPs, while the lack of any residual coordinative interaction allows the anion to explore a much greater range of orientations. In particular, in the cases examined, the anion is preferentially localized on the side of the cation closer to the coordinated Lewis base, slightly shifted toward the backside of the metallocenium cation, and farther away from the metal–methyl group. The absence of any apparent residual coordinative interaction also accounts for: (1) the observation that the diffraction-derived solid-state arrangements are unlikely to be descriptive of the solution structure in that both lattice and solvation energies must play a significant role in determining the lowest-energy configuration, (2) the expected higher polarity of these species dramatically increases their tendency to form aggregates higher than 1:1 ion-pairs.⁷⁴ Noteworthy here also are the results of quantitative NOE investigations in solution, which are in excellent agreement with the computationally optimized structures^{11a,62} for similar compounds in which the Lewis base consists of an ethylene molecule. This result is encouraging in that it implies that substitution of the olefinic substrate by a different Lewis base, incapable of undergoing

subsequent insertion, affords a good working model at least as far as solution-phase interionic structure is concerned. Further direct experimental information on cation–anion structural interactions should be accessible and should be extendable to systems in which anion effects have already been established.

Another important issue that is currently attracting much catalytic mechanistic interest is whether zirconocenium ion-pair aggregates are relevant in olefin polymerization enchainment processes.⁸ The results reported here indicate that the tendency to form aggregates is dramatically increased when the counteranion is displaced from the first coordination sphere but also confirm that only at relatively elevated concentrations (>0.5 mM) does the concentration of ion-quadruples (ca. 10%) become appreciable in nonpolar aromatic solutions. Hence, the increased tendency to form aggregates observed for ion-pairs where the counteranion is in the second coordination sphere seems thus far insufficient to consider ion-quadruples relevant under typical catalytic conditions.

Acknowledgment. This research was supported by the U.S. Department of Energy (DE-FG 02-86 ER13511) and by the MIUR (Rome, Italy, Programma di Rilevante Interesse Nazionale, Cofinanziamento 2002-2003). We thank Dr. D. Zuccaccia for helpful discussions. M.-C.C. and C.Z. thank the Dow Chemical Co. and the Italian CNR, respectively, for postdoctoral research fellowships.

Supporting Information Available: 1D Hoesy pulse sequence schematic; NMR spectra of compounds **1**, **3**, **5**, **6**, **7**, **8**, **9**, **11**, and **12**; and representative plots of PGSE data (PDF). Crystallographic data of compound **9** in CIF format. This material is available free of charge via the Internet at <http://pubs.acs.org>.

JA0387296

(74) Further investigations of aggregation as a function of temperature are required to better discriminate between predominantly enthalpically or entropically driven processes. For example, it has been reported that the enthalpy of aggregation of tetrabutylammonium chloride in chloroform is very small and that aggregation is a response to crowding in solution rather than to a favorable change in enthalpy (see ref 45b).

(75) When the motion is more rapid than molecular tumbling, the effective distance “sensed by the NOE” is $r_{\text{effective}} \geq (1/N \sum_{\mu=1}^N r_{\text{IS},\mu}^{-3})^{1/3}$. On the other hand, when the motion is slower than overall molecular tumbling, the corresponding effective distance is: $r_{\text{effective}} \geq (1/N \sum_{\mu=1}^N r_{\text{IS},\mu}^{-6})^{1/6}$ with the index μ indicating the different conformations assumed by the spin system. See: (a) Yip, P. F.; Case, D. A.; Hoch, J. C.; Poulsen, F. M.; Redfield, C., Eds. *Computational Aspect of the Study of Biological Macromolecules by Nuclear Magnetic Resonance Spectroscopy*; Plenum Press: New York, 1991, pp 317–330. (b) Tropp, J. *J. Chem. Phys.* **1980**, *72*, 6035.

(76) Macura, S.; Ernst, R. R. *Mol. Phys.* **1980**, *41*, 95.